ISTANBUL TECHNICAL UNIVERSITY ★ GRADUATE SCHOOL OF SCIENCE ENGINEERING AND TECHNOLOGY

HEAT AND MASS TRANSFER CHARACTERISTIC OF A MICRO SERPENTINE CHANNEL WITH A VISCOELASTIC COOLANT

M.Sc. THESIS

Ozan ODUNCU

Department of Aeronautics and Astronautics Engineering

Aeronautics and Astronautics Engineering Programme

MAY 2015

ISTANBUL TECHNICAL UNIVERSITY ★ GRADUATE SCHOOL OF SCIENCE ENGINEERING AND TECHNOLOGY

HEAT AND MASS TRANSFER CHARACTERISTIC OF A MICRO SERPENTINE CHANNEL WITH A VISCOELASTIC COOLANT

M.Sc. THESIS

Ozan ODUNCU
(511111132)

Department of Aeronautics and Astronautics Engineering

Aeronautics and Astronautics Engineering Programme

Thesis Advisor: Assoc. Prof. Dr. Mehmet ŞAHİN

MAY 2015

İSTANBUL TEKNİK ÜNİVERSİTESİ ★ FEN BİLİMLERİ ENSTİTÜSÜ

VİSKOELASTİK AKIŞ SOĞUTMALI MİKRO KIVRIMLI KANALLARDA AKIŞ ve ISI TRANSFERİ

YÜKSEK LİSANS TEZİ

Ozan ODUNCU
(511111132)

Uçak ve Uzay Mühendisliği Anabilim Dalı

Uçak ve Uzay Mühendisliği Programı

Tez Danışmanı: Assoc. Prof. Dr. Mehmet ŞAHİN

MAYIS 2015

Ozan ODUNCU, a M.Sc. student of ITU Graduate School of Science Engineering and Technology 511111132 successfully defended the thesis entitled **"HEAT AND MASS TRANSFER CHARACTERISTIC OF A MICRO SERPENTINE CHANNEL WITH A VISCOELASTIC COOLANT"**, which he prepared after fulfilling the requirements specified in the associated legislations, before the jury whose signatures are below.

Thesis Advisor :	**Assoc. Prof. Dr. Mehmet ŞAHİN** Istanbul Technical University	.....
Jury Members :	**Assoc. Prof. Dr. Metin MURADOĞLU** Koç University	.....
	Assist. Prof. Dr. Bayram ÇELİK Istanbul Technical University	.....

Date of Submission : **4 May 2015**
Date of Defense : **29 May 2015**

Dedicated to my family,

who offered me

unconditional love and support.

FOREWORD

I really thank to my advisor Assoc. Prof. Dr. Mehmet ŞAHİN for his help and advice in this work. I would like to thank to Assist. Prof. Dr. Bayram ÇELİK for his comments and suggestions. I would like to thank my family for their support and encouragement in my whole life. And special thanks to my sister for their endless support, understanding and encouragement. I am also grateful the use of the computing resources provided by the computing facilities at TUBITAK ULAKBIM, High Performance and Grid Computing Center.

May 2015 Ozan ODUNCU

TABLE OF CONTENTS

Page

ABBREVIATIONS

CEF	**:** Criminale-Ericksen-Filbery
CPU	**:** Central Processing Units
De	**:** Dean Number
DOF	**:** Degrees of Freedom
DSP	**:** Digital Signal Processor
FVM	**:** Finite Volume Method
GMRES	**:** Generalized Minimal Residual Method
HRV	**:** Heat Recovery Ventilation
LAPACK	**:** Linear Algebra Package
MEMS	**:** Micro Electro Mechanical Systems
MHE	**:** Microchannel Heat Exchangers
Nu	**:** Nusselt Number
Pe	**:** Peclet Number
PETSC	**:** Portable, Extensible Toolkit For Scientific Computation
Pr	**:** Prandtl Number
PTT	**:** The Phan-Thien-Tanner (PTT) Model
Re	**:** Reynold Number
SIMPLE	**:** Semi Implicit Method for Pressure Linked Equation
We	**:** Weissenberg Number

LIST OF FIGURES

Page

HEAT AND MASS TRANSFER CHARACTERISTIC OF A MICRO SERPENTINE CHANNEL WITH A VISCOELASTIC COOLANT

SUMMARY

In recent years, the microelectronic industry has shown significant improvement in terms of manufacturability, integration, functionality and enhanced performance. It has been known that microelectronic devices are strongly affected by temperature as well as thermal environment. This leads to an increasing demand for highly efficient cooling technologies. Thermal management often imposes the main obstacle for scaling down the size of modern electronic devices. Microchannel heat exchanger is an ideal candidate for small electronic devices due to their high surface-to-volume ratio as well as their small volumes. Microchannel heat sinks constitute an innovative cooling technology for the removal of a large amount of heat from a small area. Micro channels are defined as flow passages that have hydraulic diameters in the range of 10 to 100 micrometers. Following the Tuckerman and Pease (1981) at Stanford University work on single layer parallel flow micro-channel heat sink, many other studies on microchannel heat sink have been carried out. Since then, this technology has received considerable attention in microelectronics and other major application areas. Microchannel heat sinks can be used in a wide variety of applications, including electronics cooling, air-conditioning, space application, refrigeration, heat recovery ventilation (HRV), and automotive applications, to name a few.

Micro serpentine channels have been extensively used in liquid cooling due to their high heat transfer coefficients. Various enhancement methods have been proposed in order to improve the heat transfer characteristic of a microchannel. The majority of these methods share a common objective, i.e., to interrupt the boundary layer on the solid surface, and replace it with fluid from the core, thus creating a new boundary layer with an increased temperature gradient. Also, it is desirable to employ the method that gives the minimum pressure drop, and the highest heat transfer rate. In the current study, an incompressible viscoelastic fluid has been introduced as a coolant in a micro serpentine channel for heat transfer enhancement due to presence of three-dimensional purely-elastic instabilities at vanishingly small Reynolds numbers. The aim of the current study is to show that a micro serpentine channel with a viscoelastic coolant provide the higher heat transfer efficiency at vanishingly small Reynolds numbers compared to that of Newtonian flow. In order to assess the heat and mass transfer characteristics of such heat sinks, an unstructured finite volume method based on three dimensional solver has been developed. The solver utilizes a method that is based on the side-centered arrangement of flow variables with an exact mass conservation. The numerical algorithm is based on side-centered finite volume method where the velocity vector components and temperature are defined at the midpoint of each cell face while the pressure term and extra stress tensor are defined at the element centroid. The present arrangement of the primitive variables

leads to a stable numerical scheme. The resulting algebraic linear systems are solved using the FGMRES(m) Krylov iterative method with the restricted additive Schwarz preconditioner with a block-incomplete factorization within each portioned sub-domain. To speed up the iterative solver per time-step, the former solutions can be used as the initial solution. The computer program used in this study was written in Fortran. The implementation of the preconditioned Krylov subspace algorithm, matrix-matrix multiplication and the multilevel preconditioner were carried out using the PETSc (Portable, Extensible Toolkit for Scientific Computation) software package developed at the Argonne National Laboratories. The coolant, viscoelastic fluid is modeled as an incompressible Oldroyd-B fluid. The heat and mass transfer characteristic of the flow is studied numerically by varying a series of parameters such as Reynolds, Prandtl and Weissenberg numbers systematically. As the Weissenberg number is increased, the viscoelastic instability becomes significant. As a result of this, flow complexity and the strength of streamwise vortices increase. This shows not only hot fluid being transported away from the walls into the center but also the fluid near the wall continuously being refreshed. Based on initial evaluation of the present results, it is concluded that purely-elastic instabilities are responsible for heat transfer enhancement.

VİSKOELASTİK AKIŞ SOĞUTMALI MİKRO KIVRIMLI KANALLARDA AKIŞ ve ISI TRANSFERİ

ÖZET

Günümüzde imalat teknolojilerinin hızla gelişmesi mevcut cihazların giderek küçülmesine ve yeni teknolojik sistemlerin icat edilmesine sebep olmaktadır. Teknolojik gelişmelerle birlikte daha yüksek performanslı küçük boyutta cihazların yapımı gittikçe önem kazanmıştır, bu da mikro ölçekli ve hatta nano ölçekli sistemlere olan ilgiyi önemli derecede arttırmıştır. Genel olarak boyutları 1 mikrometre ile 1 milimetre arasında değişen cihazlar mikro-cihaz olarak adlandırılır. Mikro-Elektro-Mekanik Sistemler (MEMS) olarak da bilinen yeni sistemler, içerisinde akışkanın dolaştığı farklı birimleri birbirine bağlayan mikro kanallar içermektedir. Mikro kanallarda tek fazlı akış etkin bir soğutma mekanizması olarak elektronik cihazlardan reaktör soğutma sistemlerine kadar birçok alanda kullanılmaktadır.

Mikro-Elektro-Mekanik sistemlerin başlıca ilgi ve uygulama alanlarından biri olan elektronik bileşenlerin soğutulması oldukça önemlidir. Mikro elektronik aygıtlar veya sistemler çalışırken çok büyük değerlerde ısı ortaya çıkmaktadır. Mevcut soğutucular yeterli soğutma kapasitesine sahip olmadığı için MEMS teknolojisinde kullanılmamaktadır. Mikro boyuttaki kanallar küçük boyut ve ağırlıkları, dolaşan akışkan miktarının düşük olması ve yüksek ısı akıları nedeniyle MEMS teknolojisinde yoğun olarak kullanılmaktadır. Son yıllarda mikro kanallarda ısı ve kütle aktarımı önemli bir ilgi alanı olmuştur. Mikro sistemlerdeki teknolojik gelişmelere paralel olarak, mikro sistemlerde ısı ve kütle aktarımı karakteristiklerinin incelenmesi önem kazanmış ve bu konu üzerine çok sayıda deneysel ve sayısal çalışmalar yapılmıştır. Hidrolik çapı 1-100 mikrometre arasında değişen kanallar mikro kanal olarak adlandırılır. Literatürde mikro kanallardaki akış ve ısı transferiyle ilgili çok sayıda deneysel ve sayısal çalışma mevcuttur.

Isınma probleminin ortaya çıktığı önemli endüstriyel uygulamalardan biri elektronik cihazlardır. Özellikle yüksek hızda çalışan bilgisayar ve elektronik işlemciye sahip ekipmanlara ihtiyaç duyulması, bu sistemlerin ısınma problemini de beraberinde getirmektedir. Özellikle yüksek hızlı bilgisayarlarda işlemcide ortaya çıkan yüksek eklem sıcaklıkları bilgisayarın performansını ve işlemcinin ömrünü önemli ölçüde etkilemektedir. Araştırmalarda elektronik cihazlarda bozulmaya etki eden en önemli parametrenin sıcaklık olduğu gözlenmiştir. Toz, rutubet ve nem gibi etkenlerin bozulmaya etkisi sıcaklık kadar yüksek değildir.

Üretim teknolojisindeki gelişmeler, ısı değiştiricilerinin mini ve mikro boyutlarda daha yüksek hassasiyetlerde üretilmelerine olanak sağlamaktadır. Belirli geometrilerde mikro boyutlarda üretilebilen kanalların kullanımı özellikle son yirmi yıl içerisinde

oldukça yaygınlaşmıştır. Daha küçük bir yüzey alanında yüksek miktarda ve etkili ısı transferi gerçekleştirmeleri nedeniyle mikro kanallar özellikle soğutma sistemlerinde yoğun bir şekilde kullanılmakta ve performanslarının arttırılmasına yönelik çalışmalar yoğun bir şekilde devam etmektedir. Mikro kanalların yüzey alanı hacim oranı ilişkisinden dolayı büyük kanallara (mini ve makro kanallar) göre daha yüksek ısı transferi sağladığı bilinmektedir. Kanal boyutlarını küçültmenin yanında mevcut kanallarda geleneksel ısı transferi akışkanlarından farklı olarak viskoelastik akışkan kullanarak daha etkili ısı transferi elde edilebilir. Viskoelastik akışkan ile mikro kanalların performansı artırılarak ve elektronik cihazların geleneksel soğutma yöntemlerine göre etkili soğutulması planlanmaktadır.

Bu çalışmada mikro kıvrımlı kanallarda soğutucu akışkan olarak sıkıştırılamaz viskoelastik akış kullanılmış, bu akışkanın elastik kararsızlığından faydalanarak kanal içerisindeki düşük hızlara rağmen ısı transferinde artış gözlemlenmiştir. Viskoelastik akış Oldroyd-B modeli ile modellenmiştir. Newtonyen akışkanlarda ısı transferinde iyileştirme sağlayabilmek için Reynolds sayısının arttırılması gerekmektedir. Bu çalışma ile düşük *Re* sayılarında bile elastik kararsızlık sayesinde ısıl performans artışı sağlanabileceği gösterilmiştir. Mikro kanalda akış ve ısı transferini inceleyebilmek için Fortran program dilinde sonlu hacimler yöntemi ile yazılmış program kullanılmıştır. Kütlenin korunumu, momentum, Oldroyd-B ve enerji denklemleri ayrıklaştırılmıştır. Sayısal çözüm için çözüm alanı sonlu sayıda düzensiz altı yüzlü elemanlara ayrıklaştırılmış ve denklemler her bir eleman için çözülmüştür. Kenar merkezli sonlu hacim metoduna dayanan bu sayısal yöntemde hız vektör bileşenleri ve sıcaklık değerleri her bir elemanın yüzeylerinin orta noktasında tanımlanırken, basınç ve ekstra gerilme tansörü değerleri her bir elemanın merkezinde tanımlanmaktadır. Basınç, hız ve gerilme değerlerinin mevcut şekilde düzenlenmesi kararlı bir sayısal şemaya yol açar ve böylece basınç, hız ve gerilme noktalarının birbirleriyle etkileşmesi (pressure-velocity-stress coupling) için ayrıca doğal olmayan bir değişikliğe ihtiyaç kalmaz. Enerji denklemi diğer denklemlerden bağımsız olarak çözülmüştür. Hesaplanan akış profili ve hız değerleri kullanılarak sıcaklık değerleri hesaplanmıştır. Süreklilik denklemi her bir eleman içerisinde tam olarak sağlanmakta ve bu süreklilik denklemlerinin toplamı hesaplama bölgesinin sınırlarında tanımlanan küresel süreklilik denklemini vermektedir.

Zamanda birinci dereceden geri yönde farklar yöntemi ile ayrıklaştırma yapılmıştır. Küçük zaman adımlı zamana bağlı akışların çözümü için oluşan cebirsel denklemlerin çözümünde FGMRES(m) Krylov iterasyon yöntemi ön koşullandırıcı ile kullanılmıştır. Oluşan cebirsel denklemler üç ayrı matrise ayrıklaştırılmış ve bu matrislerin tersi ön koşullandırıcı olarak kullanılmıştır. Ön koşullandırılmış iteratif yöntemin ve matris işlemlerinin uygulanmasında PETSc kütüphanelerinden yararlanılmıştır. Tüm hesaplamalar 16 adet Intel(R) Xeon(R) CPU E5 – 2690, 2.90 GHz çekirdeğe sahip 6 adet bilgisayar kullanılarak yapılmıştır. Bu araştırmada yer alan tüm nümerik hesaplamalar TÜBİTAK ULAKBİM, Yüksek Başarım ve Grid Hesaplama Merkezi’nde (TRUBA kaynaklarında) gerçekleştirilmiştir. Her bir zaman adımında çözümün 96 çekirdek ile elde edilmesi yaklaşık 80 saniye sürmektedir.

Gerçekleştirilen sayısal çalışmada, Reynolds, Prandtl ve Weissenberg sayılarını sistematik bir şekilde değiştirerek mikro kıvrımlı kanal içerisinde akış ve ısı transferi incelenmiştir. *We* sayısı arttırıldığında viskoelastik kararsızlık önemli hale gelmektedir. Başka bir deyişle, kritik *We* sayısı geçildiğinde viskoelastik kararsızlık görülmektedir. Bu çalışmada viskoelastik kararsızlık incelendiğinden kritik *We* sayısından daha yüksek *We* sayılarında simülasyonlar gerçekleştirilmiştir. Bu kararsızlık akış içinde üç boyutlu akışların oluşmasına neden olmaktadır. Oluşan üç boyutlu akışların ısıtılan duvar kenarlarındaki sıcak akışkanı alıp daha soğuk olan kanalın merkezine taşımanın yanı sıra duvar kenarındaki akışkanı sürekli olarak yenilemektedir. Ayrıca oluşan üç boyutlu yapılar kanal içerisindeki karışımı arttırmaktadır. Böylece daha iyi bir ısıl performans gerçekleştirilebilmiştir. Simülasyonların sonuçlarına göre viskoelastik kararsızlık ısıl performansın artışından önemli miktarda sorumludur.

1. INTRODUCTION

1.1 Introduction

In recent years, the microelectronic industry has showed significant improvement in terms of manufacturability, integration, functionality and enhanced performance. It has been known that microelectronic devices are strongly affected by temperature as well as thermal environment. This leads to an increasing demand for highly efficient cooling technologies. Thermal management often imposes the main obstacle for scaling down the size of modern electronic devices. Microchannel heat exchanger is an ideal candidate for small electronic devices due to their high surface-to-volume ratio as well as their small volumes. Microchannels are widely used in microelectronics, and have become almost essential to modern integrated circuits like microprocessors (as shown in Figure 1.1), digital signal processor (DSPs), central processing units (CPUs), and more.

Tuckerman and Pease (1981) pioneered the research of microchannel coolant. Since that time, microchannels have received considerable attention in microelectronics. Many high flux cooling applications and industries worldwide are effectively utilizing their high heat transfer capabilities of these channels. In the automotive and aero industry, microchannels proved to be valuable in addressing the severe space

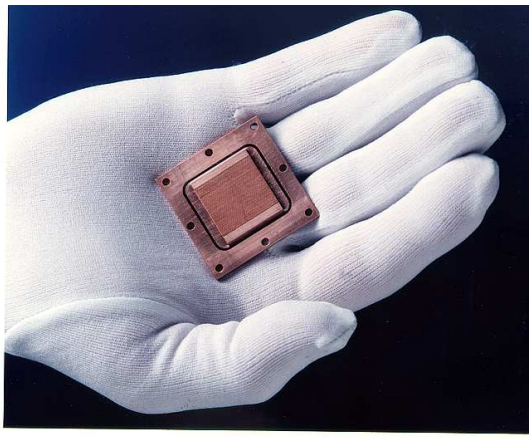

Figure 1.1: Microchannel heat processor [43].

constraints. Various passive enhancement strategies have been proposed in order to improve the heat transfer characteristic of microchannel. These strategies are as follows: wavy surfaces for channel walls [1], various aspect ratios and channel type [2], various vortex generators [3], high Reynolds number flows [2–5] and the use of viscoelastic fluids [7–10], [12–21].

Phillips [23] showed that the thermal resistance could be reduced by designing coolant which allows turbulent flow conditions. In another study, Phillips [22] showed analytically that turbulent flow should provide equivalent or better thermal performance than similar laminar flow heat sink designs. However the variation in aspect ratio and fluid velocity to achieve turbulent flow condition was limited. According to his study, the typical minimum channel widths for turbulent flow designs were in the range of 200 to 300 μm. He concluded that these large channels are much easier to manufacture than the much smaller laminar flow channel designs recommended by Tuckerman and Pease ($\approx$ 50 μm). Moreover, wavy microchannels (such as serpentine) can show enhanced performance over traditional microchannels [1]. In addition to wavy wall, the effects of vortex promoters of various shapes on heat transfer and pressure drop in microchannel was examined by Meis et al. [3]. It is concluded that better heat transfer is obtained varying the obstacle shape comparing the straight channel without obstacle. It is also found that the heat transfer as well as the pressure drop increases with decreasing channel height [2]. The flow field in sinusoidal channel is dominated by secondary flow by increasing Reynolds number in steady, incompressible fully developed flow [2–11]. These secondary flows promote convective heat transfer enhancement, resulting in high rates of heat transfer relative to fully developed flow in a straight pipe. Therefore, the establishment of secondary flows in curved passages is attracted increasing interest in microchannel flow systems as a means not only of enhancing heat transfer but also of promoting mixing. The enhancement of heat transfer due to secondary flow has been reported by a number of researchers [8–11], [16], [19]. As the dimension of microchannel is reduced, it becomes more difficult to achieve turbulent flow due to a lower Reynolds number. The present work proposes a non-traditional viscoelastic fluid as a coolant in order to create secondary flows or even viscoelastic turbulence within a microchannel at a vanishingly small Reynolds number in order to enhance heat transfer.

The viscoelastic fluids and their properties are known for a while within the non-Newtonian fluid community. These viscoelastic fluids exhibit large elastic stresses along the streamlines which lead to three-dimensional instabilities due to streamline curvature in the creeping motion of non-Newtonian polymeric liquids and are entirely absent in the corresponding motion of Newtonian liquids. Extensive reviews of viscoelastic instabilities are given by Larson [24] and Shaqfeh [25]. McKinley et al. [26] and Pakdel and McKinley [27] suggested that for shear-dominated flows one destabilizing mechanism was a combination of streamline curvature and large elastic stresses along the streamlines, giving rise to an extra *hoop stress* in a direction normal to the streamlines, which can lead to instabilities.

In the present work, we try to quantify heat transfer enhancement due to viscoelastic three-dimensional instabilities within a micro serpentine channel. The use of non-Newtonian fluids for heat transfer enhancement is not a new idea. References [7–12], [13–19] establish the connection between the enhanced heat transfer observed and the secondary flows induced by viscoelastic effects. Hartnett and Kostic [7] showed a significant enhancement of the convection coefficient for the viscoelastic fluid in a straight duct with rectangular cross section relative to the corresponding Newtonian or purely viscous fluid due to the existence of secondary flows in non-circular cross section ducts. In addition, the increase in heat transfer is primarily based on secondary flows arising from the normal force differences which do not occur in Newtonian fluids rather than natural convection. The heat transfer enhancement, however, is reduced for this type of non-Newtonian fluids (Reiner-Rivlin model and the Phan-Thien-Tanner (PTT) model) with the increase in aspect ratio because the larger aspect ratio reduces the strength of the secondary flow. The numerical method of Payvar [8] demonstrated the suitability of using that type of models to predict heat transfer to laminar flow of viscoelastic fluids in non-circular ducts. It is worth mentioning the study of Peres et al. [9] that the increase in the Nusselt number is observed with increasing the intensity of secondary flow. Furthermore, Siginer and Letelier [14] showed that increasingly large heat transfer enhancements can be computed with increasing elasticity of the fluid. As seen in Rosaguti et al. [10] and Syrjala [19], secondary flow patterns provide an increase in the rate of mixing. In other words, hot fluid is transported away from the walls into the center of the cross section with secondary flows disrupting the thermal boundary layer. As a result of the study of Naccache and Souza Mendes [16], aspect

ratio, Reynolds number, and the first normal stress difference influence the secondary flow in addition to second normal stress difference. However, the second normal stress difference plays the dominant role. In addition to those results, it is indicated that the magnitude of the secondary flow is dominated by dimensionless secondary flow coefficient (elastic behavior) and is also affected by Reynolds number (viscous behavior) [17]. In a sense, for viscoelastic fluid flows, secondary flows can develop in the absence of inertia. Moreover, despite the fact that secondary flow is weak, the heat transfer is affected by secondary flows which continuously refresh the fluid near the walls and contributes to fluid mixing. Those vortices also lead to a higher proportion of flow rate near the wall; therefore, the thermal resistance is reducing. Gao and Hartnett [18] demonstrate that the secondary flow has a major effect on the heat transfer for non-Newtonian viscoelastic fluids in laminar flow through non-circular ducts. Also, Gao and Hartnett [18] give evidence that the stronger secondary flow the higher value of the heat transfer regardless the boundary conditions on the walls.

Hartnett and Kostic [7] concluded that the dimensionless heat transfer for non-Newtonian fluids is a function of the Weissenberg number in addition to dimensionless parameters like Reynolds and Prandtl numbers in Newtonian fluids. It is well known that for low Weissenberg numbers the numerical solution converges to a steady solution as seen in [12, 13]. In addition, Galindo-Rosales et al. [13] concluded that flow patterns in microchannel showed a Newtonian like behavior at very low flow rates (low *We*), but complex non-Newtonian behavior at high flow rates (high *We*). It is also well known that viscoelastic fluid flows at low Weissenberg number develop a steady secondary flow before the onset of a purely elastic instability. In addition, high Weissenberg number is ultimately responsible for the appearance of elastic instabilities at low or even negligible Reynolds numbers in microchannels [13]. However, beyond a critical Weissenberg number purely elastic instability occurs. Therefore, the secondary vortices due to large elastic stresses along the curved streamlines are considered for a three-dimensional instability mechanism. In addition, the influence of the non-Newtonian viscosity may be seen for the fully developed laminar flow in a circular pipe, but no influence of elastic behavior even for a viscoelastic fluid appears [18]. On the contrary, in the case of non-circular channels these influences become more important, especially for viscoelastic fluids. Therefore, the results in the current study are given for beyond a critical Weissenberg numbers with rectangular cross section

to show the effects of purely elastic instability on the heat transfer enhancement. Galindo-Rosales et al. [13] experimentally identified strong secondary vortices within micro serpentine channels at low Reynolds numbers due to viscoelastic instabilities and quantified their strength. However, their effects to the heat transfer characteristics are not predicted. In the current study, initially the secondary instabilities due to viscoelastic instabilities are investigated in a micro serpentine duct with rectangular cross section and the strength of the vortices is compared with each other. Then numerical calculations are performed in order to analyze the influence of secondary flow on heat transfer enhancement.

1.2 Heat Exchanger

A heat exchanger is a device used to transfer thermal energy (enthalpy) between two or more fluids, between a solid surface and a fluid, or between solid particulates and a fluid, at different temperatures and in thermal contact, usually without external heat and work interactions. Typical applications involve heating or cooling of a fluid stream of concern and evaporation or condensation of single or multi component fluid streams, and heat recovery or heat rejection from a system. A variety of heat exchangers are used in industry and in industrial products. Heat exchangers find widespread use in power generation, chemical processing, electronics cooling, air-conditioning, food industries, space applications, refrigeration, and automotive applications. In some heat exchangers, the fluids exchanging heat are in direct contact. In other heat exchangers, heat transfer between fluids takes place through a separating wall or into and out of a wall in a transient manner. In most heat exchangers, the fluids are separated by a heat transfer surface, and ideally they do not mix. Such exchangers are referred to as direct transfer type, or simply recuperators. In contrast, exchangers in which there is intermittent heat exchange between the hot and cold fluids, via thermal energy storage and release through the exchanger surface or matrix, are referred to as indirect transfer type, or simply regenerators. Such exchangers usually have leakage fluid carryover from one stream to the other [28].

A heat exchanger consist of heat exchanging elements such as a core or a matrix containing the heat transfer surface, and fluid distribution elements such as headers, manifolds, tanks, inlet and outlet nozzles or pipes, or seals. Usually there are no

moving parts in a heat exchanger; however, there are exceptions such as a rotary regenerator (in which the matrix is mechanically driven to rotate at some design speed), a scraped surface heat exchanger, agitated vessels, and stirred tank reactors [28].

1.2.1 Classification of heat exchanger

Heat exchangers can be classified according to the following main criteria: construction type, heat transfer mechanisms, heat transfer processes, number of fluids, flow arrangements, and surface compactness as shown in Figure 1.2.

Another arbitrary classification can be made based on the heat transfer surface area to volume ratio. Heat exchangers in terms of types and size are available in many varieties. Some of the prevalent types are; shell and tube heat exchangers, plate-fin heat exchangers, plate heat exchangers, and the heat exchanger used in the current study; microchannel heat exchanger.

In order to make the best selection of heat exchanger, it is important to have some knowledge of the different types of heat exchangers and how they operate. Also, one must take into consideration the total cost of the equipment which includes purchase, operating and maintenance.

1.2.1.1 Shell and Tube heat exchanger

This exchanger is generally built of a bundle of round tubes mounted in a cylindrical shell with the tube axis parallel to that of the shell as shown in Figure 1.3. One fluid flows inside the tubes, and the other flows over the tubes to transfer heat between the two fluids. A variety of different internal constructions is used in shell and tube exchangers, depending on the desired heat transfer and pressure drop performance, contain operating pressures and temperatures, and so on. The shell and tube heat exchanger are widely used in industry because of allowing for a wide range of pressures and temperatures and most versatile in terms of type. On the contrary, lower heat transfer efficiency and more space requirement consist of two main disadvantages.

1.2.1.2 Plate heat exchanger

Plate type heat exchangers are usually built of several layers of thin plates stacked in contact with each other, and the two fluids made to flow separately along adjacent channels. This type has an advantage over the other heat exchangers, since the fluid

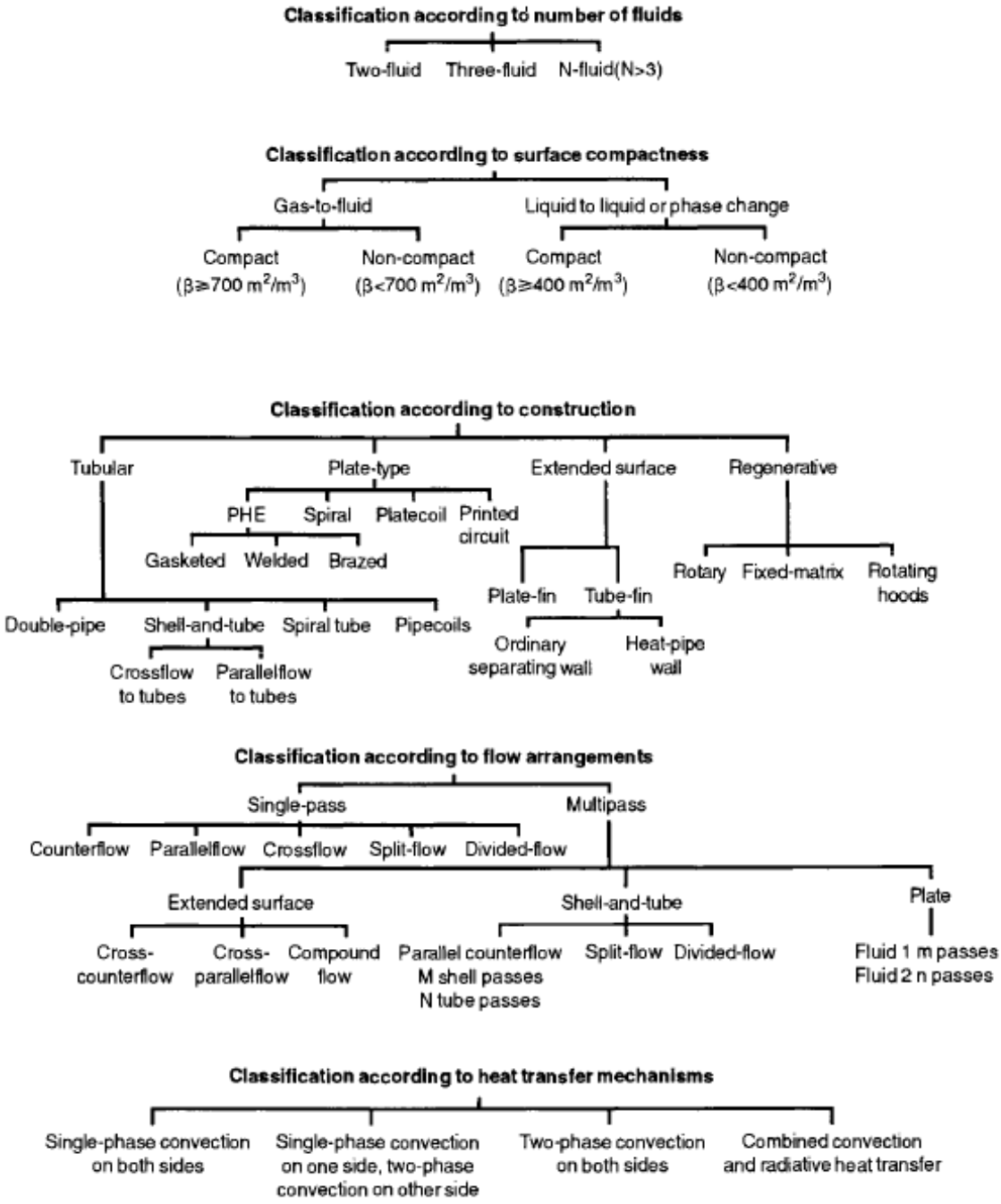

Figure 1.2: Classification of heat exchangers [28].

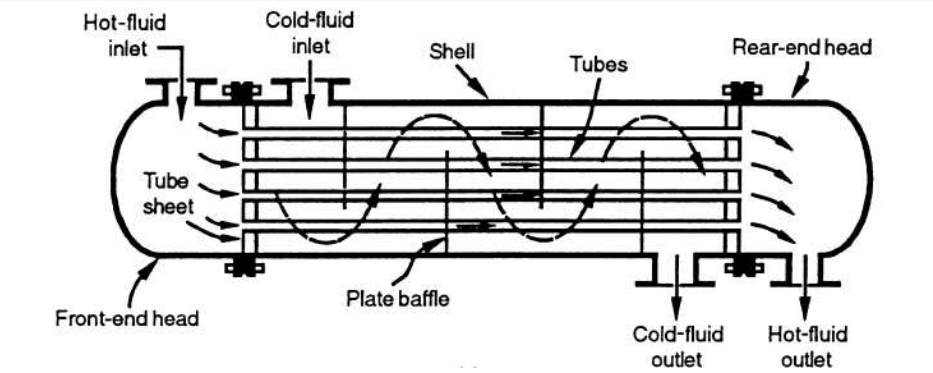

Figure 1.3: Shell and Tube heat exchanger [28].

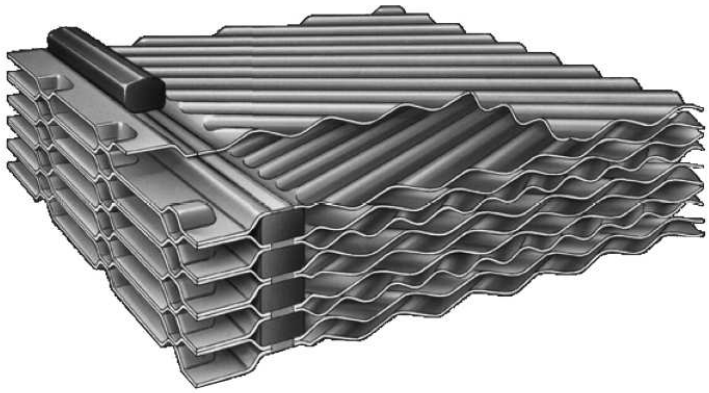

Figure 1.4: Section of a welded plate heat exchanger [28].

is exposed to a large surface area that will result in enhanced heat transfer efficiency. Many fins configurations can be used with this heat exchanger such as straight fins, louvered fins, strip fins, offset fins, and wavy fins. A pack of plates for a conventional plate and frame exchanger is shown in Figure 1.4.

1.2.1.3 Extended surface heat exchangers

One of the most common methods to increase the surface area and exchanger compactness is to add the extended surface (fins) and use fins as high as possible on one or both fluid sides, depending on the design requirement. Addition of fins can increase the surface area. The resulting exchanger is referred to as an extended surface exchanger. The heat transfer coefficient on extended surfaces may be higher than that on unfinned surfaces. The structure of plate fin heat exchanger is shown in Figure 1.5.

1.2.1.4 Indirect or direct contact heat exchangers

In an indirect contact heat exchanger, the fluid streams remain separate and the heat transfers continuously through an impervious dividing wall. Thus, there is no direct contact between thermally interacting fluids. On the contrary, in a direct contact exchanger, two fluid streams come into direct contact, exchange heat, and are then separated. As comparing indirect one, high heat transfer rates and relatively cheaper the exchanger construction are achievable.

1.2.1.5 Regenerators

The regenerator is a storage type exchanger where heat from the hot fluid is intermittently stored in a thermal storage in a packing before it is transferred to the cold

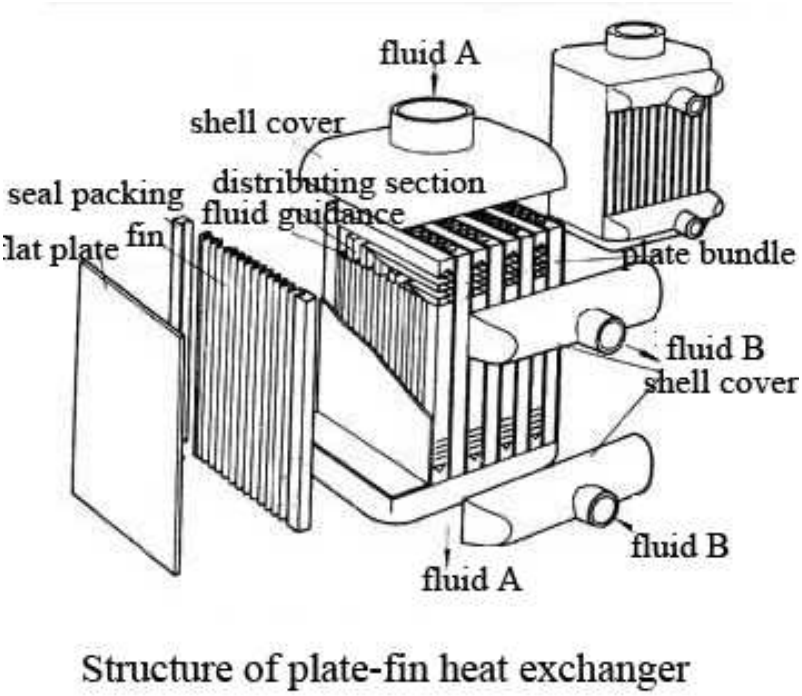

Figure 1.5: Structure of plate-fin heat exchanger [44].

fluid. In regenerators, the hot and cold fluids pass simultaneously through different but adjacent channels.

1.2.1.6 Compact heat exchanger

Compact heat exchangers are characterized by a large heat transfer surface area per unit volume of the exchanger, resulting in reduced space, weight, support structure and energy requirements and cost. The meaning of compactness is illustrated in Figure 1.6. High heat transfer coefficients are achievable with small hydraulic diameter flow passages with gases, liquids, and two-phase flows. Many different configurations are available. Contrary, material of construction selection is critical due to thin wall thickness. Compact heat exchanger also works narrower range of pressure and temperature. An example of compact heat exchangers is shown in Figure 1.7.

1.2.2 Micro heat exchanger

In recent years, the microelectronic industry has showed significant improvement. It has been known that microelectronic devices are strongly affected by temperature as well as thermal environment. Heat generated by electronic devices must be dissipated to improve reliability and prevent premature failure. This leads to an increasing demand for highly efficient cooling technologies.

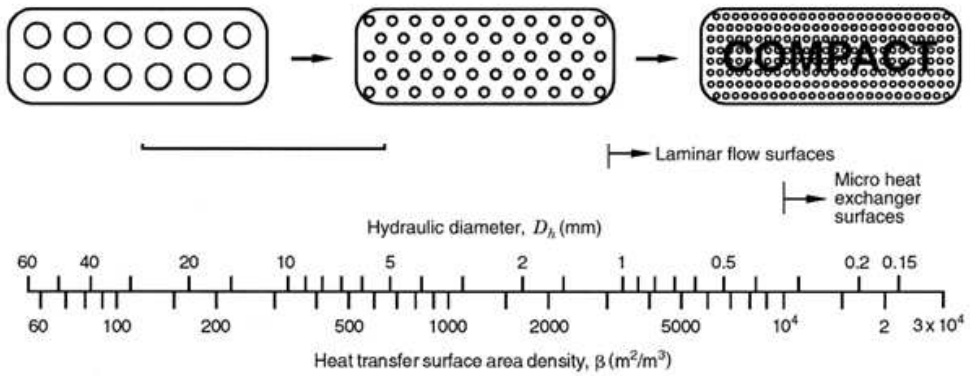

Figure 1.6: Heat transfer surface area density spectrum of exchanger surfaces [28].

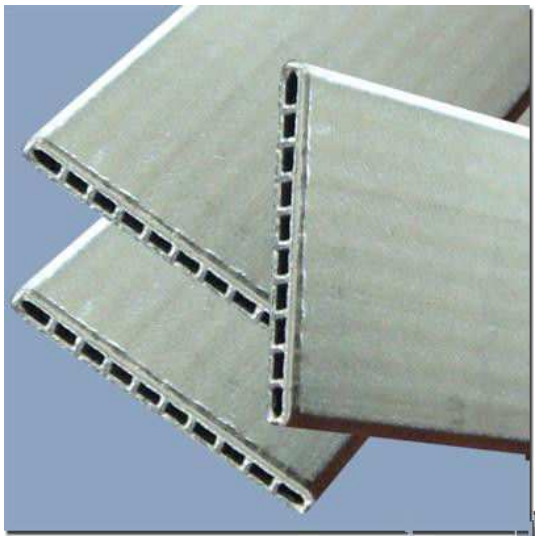

Figure 1.7: The microchannels (compact heat exchanger) [45].

Microprocessors and power handling semiconductors are examples of electronics that need a heat sink to reduce their temperature through increased thermal mass and heat dissipation primarily by conduction and convection. Microchannel heat sinks constitute an innovative cooling technology for the removal of a large amount of heat from a small area. Microchannel heat sinks combine the attributes of very high surface area to volume ratio, large convective heat transfer coefficient, small mass and volume. In common use, it is a metal object brought into contact with an electronic component's hot surface, though in most cases, a thin thermal interface mediates between the two surfaces. Heat sinks are widely used in electronics, and have become almost essential to modern integrated circuits like microprocessors, DSPs, central processing units (CPUs), and more.

A heat sink usually consists of a metal structure with one or more flat surfaces to ensure good thermal contact with the components to be cooled, and an array of comb or fin to

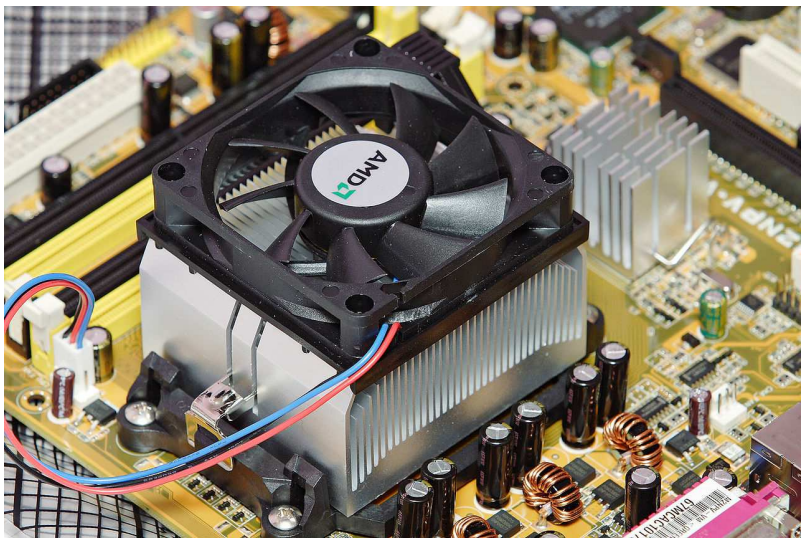

Figure 1.8: Heat sink and fan over processor [46].

increase the surface contact with the air, and thus the rate of heat dissipation. A heat sink is sometimes used in conjunction with a fan to increase the rate of airflow over the heat sink as shown in Figure 1.8. This maintains a larger temperature gradient by replacing warmed air faster than convection would.

Microchannel heat exchangers (MHEs) are an ideal candidate for small electronic devices. In a microchannel heat exchanger, multiple microchannels are stacked together as shown in Figure 1.9 in order to increase the total contact surface area for heat transfer enhancement and reduce the total pressure drop by dividing the flow among many channels. The high cooling capability of microchannel heat sinks is both due to the large extended surfaces of microchannel over its volume but also due to the small size of the microchannels. Thus, the heat transfer coefficient is very high in microchannels. Many high flux cooling applications and industries worldwide, varying from space, energy, heating, ventilation and air conditioning, and transportation are effectively utilizing their high heat transfer capabilities of these channels.

The distinguishing feature of microchannel heat sinks is the size of their cooling channels. Microchannels offer advantages due to their high surface-to-volume ratio (as seen in Figure 1.9) and their small volumes. The large surface-to-volume ratio leads to high rate of heat and mass transfer, making micro devices excellent tools for compact heat exchangers. In addition, the reduction of volume and weight and increase in mobility and use are another advantages of micro heat exchanger. Tuckerman and Pease (1981) pioneered the research of microchannel coolant, heat sink. Since then, microchannels have received considerable attention in microelectronics and other

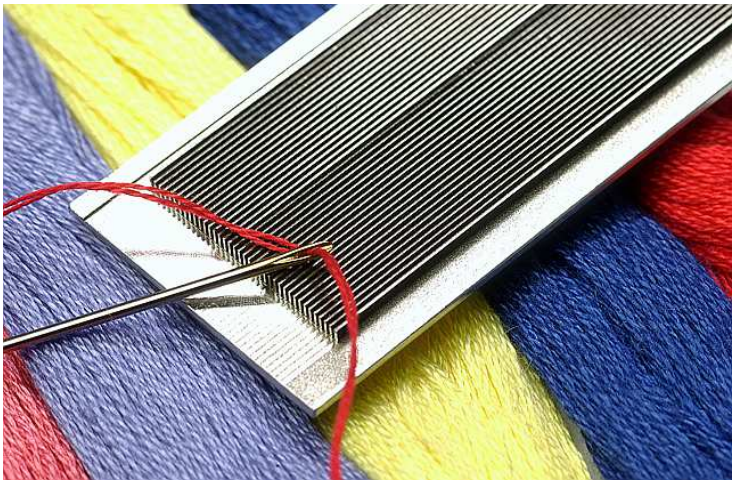

Figure 1.9: Microchannels [43].

application areas. Their studies motivated many researchers to examine further the use of microchannels in heat transfer systems. The study of Phillips [23] in 1988 showed that the thermal performance of microchannel heat sinks was approximately two orders of magnitude better than the thermal performance of other devices used to cool microelectronic devices at that time. Nowadays microchannel heat exchangers have been known as having high performance due to the very small channel diameter and enhanced surface area.

There is no universal agreement on size classification convention. The following is a popular size classification [29]. This classification is based on the dimensions of the channels.

For flow channels,

$$D_H = 10 - 100 \quad \mu m, \quad microchannels,$$

$$D_H = 100 \quad \mu m - 1 \quad mm, \quad minichannels,$$

$$D_H = 1 - 3 \quad mm, \quad macrochannels,$$

$$D_H > 6 \quad mm, \quad conventional\ channels.$$

For heat exchangers,

$$D_H = 1 - 100 \quad \mu m, \quad micro\ heat\ exchangers,$$

$$D_H = 100 \quad \mu m - 1 \quad mm, \quad meso\ heat\ exchangers,$$

$$D_H = 1 - 6 \quad mm, \quad compact\ heat\ exchangers,$$

$$D_H > 6 \quad mm, \quad conventional\ heat\ exchangers.$$

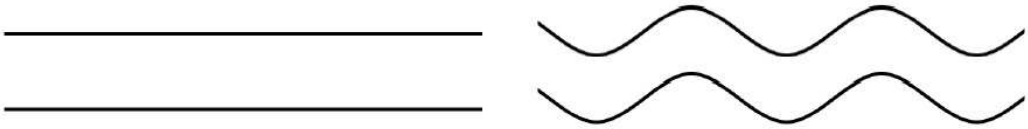

Figure 1.10: Left: Planar channel Right: Sinusoidal (serpentine) channel.

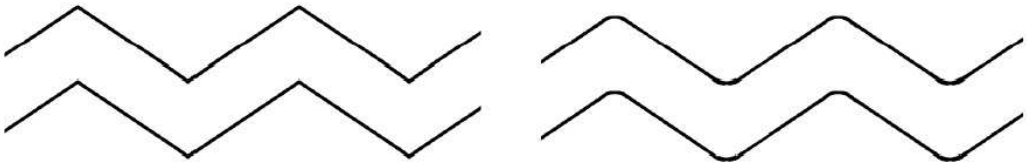

Figure 1.11: Left: Corrugated channel Right: Corrugated channel with rounded corners.

Many different types of geometries have been used in heat exchangers and subsequently studied numerically and experimentally. For this thesis the serpentine wavy channel is used, but a review of all types of geometries is helpful when designing new geometries. Figure 1.10 shows the two types of channels, planar and sinusoidal (also called serpentine). Figures 1.11 and 1.12 show other common geometries [30].

1.2.3 The Thermal performance of microchannels heat exchangers

The general function of a heat exchanger is to transfer of thermal energy from one fluid to another. Also, heat sinks are designed to dissipate as much heat as possible from such as electronic devices. The straight forward purpose of heat exchangers is controlling a system temperature by removing thermal energy. This is crucial to reduce overheating of devices and to increase the endurance and sustainability of devices.
Micro heat exchangers are used in many fields of technology; therefore, the design of heat transfer devices as well as the heat transfer is an important issue. Thermal and fluid performance for microchannel heat sinks can be modeled with Reynolds numbers, friction factors, Nusselt numbers, and parameters that describe the thermal and fluid performance of the coolant [23]. In addition, the thermal performance of a heat sink is often specified in terms of its total thermal resistance. It is desired that the thermal

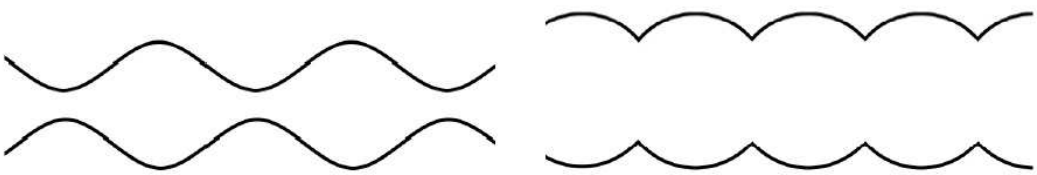

Figure 1.12: Left: Bellowed channel Right: Arc-shaped bellowed channel.

resistance is kept as low as possible. Low thermal resistance is achieved for heat sinks using high thermal conductivity material, narrow heat flow distance and large surface area for heat flow. Heat sinks are designed using high thermal conductivity material with fins offering extended surfaces to enhance the heat removal from heat generating components. Both high thermal conductivity and increased cooling surface area will reduce the total thermal resistance of the heat sink and thus effective cooling of electronic devices is achieved. Therefore, the removal of heat from devices can be maximized if the thermal resistance of the cooling system is kept as minimum as possible.

The dimensions of microchannel and the fluid flow property influence the cooling capability of the microchannel system. In addition, the microchannel geometry, size, and type such as wavy have significant impact on the performance of heat exchanger. Therefore, there will be great significance to explore the optimal structure of microchannel during the microchannel heat exchanger design. The microchannel heat sink is defined by some physical parameters such as length, width, aspect ratio, fin width, and height of channel, to name a few. By controlling these physical parameters as well as external parameters such as pumping power, better heat transfer performance can be obtained.

The thermal and fluid performance characteristics of a coolant depend on whether the coolant flow is laminar or turbulent [23]. The Reynolds number which is the ratio of inertial forces to viscous forces can be used to estimate the transition between laminar and turbulent flow. Phillips [23] showed analytically that turbulent flow should provide equivalent or better thermal performance than similar laminar flow heat sink designs. The typical minimum channel widths for turbulent flow designs were in the range of 200 to 300 μm [22]. In general, the rate of heat transfer increases as the coolant velocity increases. In the study of [2, 3, 5, 11, 17, 18], a higher average Nusselt number is obtained as Reynolds number increases. However, as the coolant velocity increases, the coolant pressure drop also increases, and greater pumping power is necessary [1–3, 10, 11]. In addition to that reason, it is shown that pressure drop, an important parameter for microchannel heat sink design, is a strong function of the channel geometry in the study of Upadhye and Kandlikar [31]. The increase of pressure drop depends on whether the channel's width larger or smaller. A narrow and deep channel is better than having a wide and shallow channel with regard to

both heat transfer and pressure drop [31]. However, increasing the channel depth any further does not substantially reduce the pressure drop. Therefore, the primary goal is the design of a microchannel heat exchanger that the highest heat transfer rate can be achieved with the lowest possible pressure drop. Secondary goals include ease of manufacturability and maintenance. Thus, before designing the microchannel, the pressure loss and heat transfer characteristics must be accurately predicted. In order to design and fabricate such micro devices effectively, the fluid flow on the micro scale must be better understood. As the field of micro devices continues to grow, the knowledge of micro scale fluid flow mechanism is becoming increasingly important. A comprehensive study of the results of micro scale single phase internal flows has been compiled by Papautsky and Ameel [32].

There have been a lot of researches in order to improve the thermal performance of microchannel heat exchanger including wavy wall, aspect ratios, channel types, viscoelastic fluids and vortex creators, to name a few. Wavy channels have been investigated to improve the heat transfer performance of laminar fluid flow applied to microchannel heat sinks. In the study of Gong et al. [1], parametric study of three dimensional laminar fluid flow and heat transfer characteristics in micro sized wavy channels was performed by varying the wavy feature amplitude, wavelength, and aspect ratio for different Reynolds numbers. As a result of this study [1], wavy microchannels can show enhanced performance over traditional microchannels, and can be an attractive choice for cooling of future microelectronics in low *Re* laminar flow. In addition to wavy wall, vortex promoters in straight channel have been examined by many researchers to increase heat transfer. Meis et al. [3] examined the effects of vortex promoters of various shapes on heat transfer and pressure drop in microchannel. Better heat transfer is obtained varying the obstacle shape comparing the straight channel without obstacle. Considering elliptical, rectangular, and triangular obstacles at varying aspect ratios shows that the triangle obstacle provides best results, then the rectangles, then the ellipses, and that the performance is improved as the aspect ratio is decreased [3]. However, triangles, ellipses and too slender rectangles should be disregarded due to practical micro manufacturing. The effect of channel heights on heat transfer was investigated for serpentine or corrugated channel over a range of Reynolds numbers by Volker and Vanka [2]. It was concluded that the Nusselt number as well as the friction factor depends linearly

on the Reynolds number. Volker and Vanka [2] found a significant increase in heat transfer for higher Reynolds numbers. It is also found that the heat transfer as well as the pressure drop increases with decreasing channel height. In addition to that study, the flow field in sinusoidal channel is dominated by secondary flow by increasing both Reynolds number and amplitude to half wavelength ratio with regard to Rosaguti et al. [10] in steady, incompressible fully developed flow. These secondary flows promote convective heat transfer enhancement, resulting in high rates of heat transfer and low pressure loss relative to fully developed flow in a straight pipe. The establishment of secondary flows in curved passages is attracted increasing interest in microchannel flow systems as a means not only of enhancing heat transfer but also of promoting mixing.

The use of non-Newtonian fluids for heat transfer enhancement was introduced by Hartnett and Kostic [7] at first. Numerical investigations in rectangular cross-sections of Gao and Hartnett [17, 18], Peres et al. [9], Galindo-Rosales et al. [13], Siginer and Letelier [14, 15], Naccache and Souza Mendes [16], Rosaguti et al. [10, 11], Poole et al. [12] and Syrjala [19] establish the connection between the enhanced heat transfer observed and the secondary flows induced by viscoelastic effects. Gao and Hartnett [7] showed a significant enhancement of the convection coefficient for the viscoelastic fluid in a straight duct with rectangular cross section relative to the corresponding Newtonian or purely viscous fluid due to the existence of secondary flows in non-circular cross section ducts. The increase in heat transfer is primarily based on secondary flows arising from the normal force differences which do not occur in Newtonian fluids. The study of Peres et al. [9] observed the increase in the Nusselt number with increasing the intensity of secondary flow. The influence of the second normal stress coefficient, the Reynolds number, and the aspect ratio on the heat transfer was considered with elastic non-Newtonian fluids in steady laminar flow through rectangular ducts in study of Gao and Hartnett [18]. As a result of this study, the heat transfer increases as the aspect ratio increases due to the secondary flow. However, the influence of aspect ratio is complicated because the change of geometry affects both the distribution and the magnitude of secondary flow. Moreover, Gao and Hartnett [18] found that the secondary flow results in a significant increase in the heat transfer, especially for aspect ratios of 0.5 and 1.0. Galindo-Rosales et al. [13] experimentally identified strong secondary vortices within micro serpentine channels

at low Reynolds numbers due to viscoelastic instabilities. According to the results of these studies, in this paper we investigate the effect of viscoelastic there dimensional instabilities within a serpentine microchannel on the heat transfer enhancement.

1.3 Organization of The Thesis

The thesis consists of five chapters with the first chapter gives the introduction of the thesis, overview of the heat exchanger and the organization of the thesis. The literature review on microchannel flow including the experimental, analytical and numerical studies are provided in chapter two. In chapter three, conservation of mass, momentum, heat equations and the constitutive equation for Oldroyd-B model for the incompressible flows of a non-Newtonian fluid are given. The integral form of these equations is shown. Then, the three-dimensional numerical discretization along *x*-,*y*- and *z*- directions is provided. In addition, boundary conditions used in numerical simulation and their integral form are given. The pressure drop and heat transfer characteristics of microchannel heat sink are numerically analyzed in chapter four. The simulations are performed with the code written using Fortran computer programming language. The simulations are performed with Newtonian and Oldroyd-B fluids. The results of these simulations and heat transfer analysis are presented. In the last section, chapter five, the conclusions of present work is given and the recommendations for future work are pointed out.

2. LITERATURE REVIEW

For the last three decades, there has been an increasing interest in the area of microchannel flow and heat transfer due to the high rates of heat transfer. In the literature, there are numbers of publications concerning heat transfer enhancement in microchannels. In this chapter, the works on microchannel flow including the experimental, analytical and numerical studies are reviewed.

Gong et al. [1] investigated wavy channels to improve the heat transfer performance of laminar fluid flow applied to microchannel heat sinks. Parametric study of three-dimensional laminar fluid flow and heat transfer characteristics in micro sized wavy channels was performed by varying the wavy feature amplitude, wavelength, and aspect ratio for different Reynolds numbers between 50 and 150. Their study aimed to find out whether there was a possibility for improving the heat transfer using wavy microchannels without having a significant rise in the pressure drop or not. It was found that in wavy channels, no vortical structure, i.e. the existence of secondary flow, could be observed not only due to low *Re* numbers also low wave amplitude. In contrast, the maximum wall temperature decreased due to vortex generation as wave amplitude, *Re* and aspect ratio varying from 1 to 2.5 increased and wavelength decreased. Moreover, the negative effect of increase in pressure drop for channels with higher amplitudes was overcome by the more dominant positive effect of increase in heat transfer at high *Re*, resulting in an improved overall performance. In a similar way, the negative effect of increase in pressure drop for channels with both lower wavelengths and higher aspect ratios was overcome by the more dominant positive effect of increase in heat transfer at high *Re*. In addition, a significant increase in the pressure drop could be seen although flow recirculation existed in channel with high wave amplitude. Similarly, the pressure drop increased considerably with aspect ratio when *Re* is kept the same. The high pressure drop is still problem in microchannels and leads to an increase in pumping power. Based on the comparison with straight channels, it was found that wavy channels could provide improvement overall thermal performance. Therefore, wavy microchannels could show enhanced performance over

traditional microchannels, and could be an attractive choice for cooling of future microelectronics in low *Re* laminar flow.

Volker and Vanka [2] investigated fluid flow, heat transfer and pressure drop of the two dimensional serpentine or corrugated channel over a range of Reynolds numbers between 175 and 725 for three different channel heights (*H*). The results of the numerical computations for both steady and unsteady flow were shown in their study. Firstly, solutions for Reynolds numbers of 215, 315, 525 and 700 were computed for the channel height of 1.3. They could say that the observed pattern of vortex formation and dissipation existed for all Reynolds numbers at which the flow was unsteady. The flow was subject to a single oscillatory mode for a Reynolds number of 215. Only a limited increase in heat transfer was observed despite the flow being unsteady. Moreover, at a Reynolds number of 315, in addition to the primary mode of oscillation secondary modes appeared in the velocity time signal. The occurrence of secondary modes resulted in a significant increase in the rate of heat transfer. Furthermore, for the higher Reynolds numbers, vortex generation and dissipation allowed for more than one vortex to be trapped in the cavities at one instant in time. They also found that the vortices grew bigger with increasing Reynolds number. Thus, the rate of heat transfer was almost four times as high as the rate of heat transfer in the straight channel for a Reynolds number of 700. The second channel height of 1.6 was investigated in their study. For all the Reynolds numbers studied the flow was subject to a single mode of oscillation. Unlike for the former conclusion, it could be seen that even at the higher Reynolds numbers the flow path was significantly less obstructed by vortices ejected from the bends. Hence, there was only little interaction between the individual vortices. A third set of computations was carried out for a spacing of 1.0 unit between upper and lower walls. Unlike for the previously mentioned case of a channel height of 1.6 units, multiple modes of oscillation were present even for the smallest investigated Reynolds number of 340. The oscillations became more violent with increasing Reynolds number. They observed significant vortex interactions, which caused multi frequency oscillation patterns in the velocity time signals. In the periodic case, it was concluded that the Nusselt number as well as the friction factor depended linearly on the Reynolds number. They found a significant increase in heat transfer for higher Reynolds numbers. It was also found that the heat transfer as well as the pressure drop increased with decreasing channel height.

Meis et al. [3] conducted numerical study of the effects of heat transfer and pressure drop produced by vortex promoters of various shapes in two-dimensional, unsteady, laminar flow in a straight microchannel. Three reference cross sections, namely circular/elliptical, rectangular, and triangular, at various aspect ratios were considered in terms of heat transfer enhancement as a result of different vortex structure created by them. The effect of the blockage ratio, the Reynolds number, and the relative position and orientation of the obstacle were also studied. It was intended to obtain useful design criteria of micro-cooling systems, taking into account that practical solutions should be both thermally efficient and not expensive in terms of the pumping power. That is, heat transfer rate enhancement and the pressure drop increase must be considered together to evaluate the efficiency. Heat transfer in these systems could be enhanced by vortex promoters (built-in obstacles in the microchannels) since they produce transversal convection which is a quite effective heat transport mechanism if the produced vortices exhibit appropriate size and intensity. Considering elliptical, rectangular, and triangular obstacles at varying aspect ratios showed that the latter provided best results, then the rectangles, then the ellipses, and that the performance was improved as the aspect ratio decreasing. However, triangles, ellipses and too slender rectangles should be disregarded due to practical micro manufacturing. It was concluded that thermal efficiency either remained constant or slightly increased as the *Re* number increases in comparison with mechanical penalty, i.e. pumping power, always increasing. Therefore, increasing the *Re* number did not seem to be a good way to improve performance. On the other hand, the choice of low *Re* number could be a convenient way to increase performance due to low pumping power.

Toh et al. [4] investigated the three-dimensional fluid flow and heat transfer phenomena inside heated microchannels. The steady, incompressible, laminar flow and heat transfer equations were solved using a finite volume method. The vertex based FVM is chosen. The numerical computation was confirmed by comparing the predicted local thermal resistances with available experimental data. It was found that the heat input lowered the frictional losses, particularly at lower Reynolds numbers. It was found that at lower Reynolds numbers the temperature of the water increased, leading to a decrease in the viscosity and hence smaller frictional losses.

Qu and Mudawar [5] analyzed the three-dimensional fluid flow, pressure drop and heat transfer characteristics in rectangular microchannel heat sink using water as

the cooling fluid both experimentally and numerically. To solve the Navier-Stokes and energy equations, they used the finite difference method and SIMPLE algorithm with steady, incompressible and laminar flow. Their numerical results were compared with analytical solutions and available experimental data. They founded that the temperature rose along the flow direction in the solid and fluid regions could be approximated as linear. In addition, it could be seen that the average temperatures decreased with increasing Reynolds number and the differences between the temperature gradients at the channel inlet and outlet were more apparent at high Reynolds numbers. Moreover, as Reynolds number increases, a higher average Nusselt number was obtained at a given longitudinal distance. They also found that the flow developing region was affected by the Reynolds number. It was mentioned that fully developed flow might not be achieved inside the heat sink for high Reynolds numbers. In another study of Qu and Mudawar [6], the pressure drop and heat transfer characteristics of a single-phase microchannel heat sink were investigated both experimentally and numerically. The measured pressure drop and temperature distributions within the heat sink show good agreement with the corresponding numerical predictions. These findings are focused on general characters of heat transfer and flow in microchannels heat sink and concluded that conventional Navier–Stokes and energy equations can adequately predict the fluid flow and heat transfer characteristics of microchannel heat sinks.

Hartnett and Kostic [7] performed an experimental study and showed a significant enhancement of the convection coefficient for the viscoelastic fluid in a straight duct with rectangular cross-section relative to the corresponding Newtonian or purely viscous fluid due to the existence of secondary flows in non-circular cross section ducts. It is also known that elastic properties of viscoelastic fluid do not play significant role in fully developed pipe flow. The elasticity of the viscoelastic fluids was measured as a function of shear rate using dimensionless Weissenberg number. In addition, the weak secondary flow had a larger influence upon the heat transfer behavior than on the fluid dynamics. The increase in heat transfer was primarily based on secondary flows arising from the normal force differences which do not occur in Newtonian fluids rather than natural convection. They pointed out that if this was correct then the dimensionless heat transfer was a function of the *We* number in addition to usual dimensionless parameters like Reynolds and Prandtl numbers applying to

Newtonian fluids. The heat transfer enhancement, however, is reduced for this type of non-Newtonian fluids (Reiner-Rivlin model and the Phan-Thien-Tanner (PTT) model) with the increase in aspect ratio because the larger aspect ratio reduces the strength of the secondary flow.

In the study of Payvar [8], a realistic prediction of laminar flow heat transfer to viscoelastic fluids must be based on a model more complex than a purely viscous non-Newtonian flow as a result of the absence of reliable methods for the accurate prediction of heat transfer in a laminar flow of non-Newtonian fluids through rectangular ducts. The numerical method of Payvar [8] demonstrated the suitability of using constitutive equations which take into account non-zero normal stress coefficients for laminar heat transfer prediction of viscoelastic fluids by comparing experiments of Hartnett and Kostic [7]. In addition, Payvar [8] established the connection between the enhanced heat transfer observed and the secondary flows induced by viscoelastic effects.

Peres et al. [9] carried out an investigation on convective heat transfer with viscoelastic fluids in a rectangular duct to analyze the influence of secondary flow on heat transfer enhancement. In their study, the Phan-Thein-Tanner constitutive equation with non-zero second normal-stress difference was used for simulations. In addition, the duct had an aspect ratio of 2 as a result of the larger aspect ratio reducing the strength of the secondary flow. The numerical results were validated by comparing with the experimental heat transfer data of Hartnett and Kostic [7]. Their simulations showed an enhancement of heat transfer for viscoelastic fluids. The enhancement based on the fluid rheology, particularly the shear-thinning nature of the viscoelastic fluid and the existence of the secondary flow induced by the non-zero second normal stress differences. Also, the increase in the Nusselt number was observed with increasing the intensity of secondary flow. Moreover, despite the fact that secondary flow was weak, the heat transfer was affected by vortices which continuously refresh the fluid near the walls and contributes to fluid mixing. Those vortices also led to a higher proportion of flow rate near the wall; therefore, the thermal resistance is reducing. Another result of their study for fluids with a strong secondary flow effects was that buoyancy will not enhance the global heat transfer, but essentially redistributes it.

Rosaguti et al. [10] studied the effect of Reynolds and Prandtl numbers on fully developed laminar flow, heat transfer enhancement and relative pressure drop penalty

in periodic serpentine channel with a semi-circular cross-section for the constant wall heat flux ($H2$) and constant wall temperature (T) boundary conditions. They assessed the performance of the serpentine channel by comparing pressure drop and rate of heat transfer to the same quantities arising in fully developed flow in a straight pipe. The flow in channels was characterized by the formation of Dean Vortices. The Dean number giving a measure of the importance of inertial and centrifugal forces relative to viscous forces is directly proportional to the Reynolds number. It found out that the establishment of Dean Vortices at the bends gives rise to significant heat transfer enhancement which, in the absence of the creation of recirculation zones, could be achieved with a very small relative pressure drop penalty. It found out that the flow at low Reynolds number smaller than 50 not only acts to suppress secondary flow formation as the viscous forces are large in comparison with inertial forces, also tends towards the straight pipe solution. In consequence of this, flow and heat transfer remain close to the straight pipe solution. As the Reynolds number was increased further, inertial forces became significant. As a result of this, flow complexity, as well as the number and strength of vortices, increases. Moreover, more complex secondary flow patterns emerge and the flow domain becomes increasingly dominated by these vortices leading to efficient fluid mixing and high rates of heat transfer. This shows hot fluid being transported away from the walls into the center of the cross section, with secondary flows disrupting the thermal boundary layer. In addition, the heat transfer coefficient and friction factor increase relative to their values in straight sections. Finally, it was concluded that the serpentine channel with semi-circular cross-section generates greater flow complexity. Furthermore, high rates of heat transfer and low pressure loss were found relative to fully developed flow in a straight pipe, with heat transfer enhancements greater than 10 for a Prandtl number of 100.

In another study, Rosaguti et al. [11] investigated the effect of Reynolds number and amplitude to half wavelength ratio (A/L) on heat transfer enhancement and pressure drop for steady, incompressible fully developed laminar flow and heat transfer with streamwise periodic sinusoidal channels. They applied the same boundary conditions as their previous study [10]. If the results are examined in more detail, higher values of A/L give steadily greater heat transfer enhancement, while the relative pressure drop becomes quite insensitive to A/L when A/L is greater than 0.333. The thermo-hydraulic performance results in increase of the efficiency with both Reynolds number and

amplitude to half wavelength ratio up to $Re \approx 175$. However, the heat transfer enhancement at higher Reynolds number rises relatively faster. Moreover, only a single pair of vortices was generated in channel, with no observable bifurcation in the vortex structure for Reynolds numbers up to 200. Like the former study, it was concluded that the flow field in the sinusoidal geometries was increasingly dominated by secondary flow structures (Dean Vortices) with increasing *Re* number and *A/L*. These vortices promoted convective heat transfer enhancement, resulting in high rates of heat transfer and low pressure loss relative to fully developed flow in a straight pipe.

Poole et al. [12] performed a detailed numerical investigation of inertialess viscoelastic fluid flow through three-dimensional serpentine channels of varying radius of curvature and aspect ratio using the Oldroyd-B model which predict a zero second normal stress difference. The effects of radius of curvature, aspect ratio and solvent-to-total viscosity ratio on the strength of the secondary flow were investigated. In their numerical method, the governing equations were solved using a time-marching implicit finite volume method. It is well known that for low Weissenberg numbers the numerical solution converges to a steady solution, in other words, creeping viscoelastic fluid flows through such serpentine channels at low *We* number develop a steady two-dimensional flow. However, beyond a critical *We* number a time-dependent three-dimensional purely elastic instability occurs. Therefore, the results in the current study [12] were restricted to *We* numbers below the occurrence of this purely elastic instability; thus, the flow remained steady. As a result of study ($We = 0.2$), the streamwise velocity component (u) was the only non-zero component in the total absence of inertia for the Newtonian fluid. The transverse (v) and spanwise (w) velocities were zero. On the other hand, for the viscoelastic fluid, a weak secondary flow was clearly apparent although the streamwise velocity contours were qualitatively similar. The secondary flow strength dominated by the transverse component was shown to be a function of a modified Deborah number over a wide parameter range. Their study revealed the existence of a secondary flow which is absent for the equivalent Newtonian fluid flow. The secondary flow arose due to the curvature of the geometry and the streamwise first normal stress differences generated in the flowing fluid and could be thought of as the viscoelastic equivalent of Dean vortices.

Galindo-Rosales et al. [13] reviewed an experimental work by the topic of elastic instabilities in flow having a strong extensional component. In addition, this

work summarized five experimental investigations on pressure driven flows in micro-geometries that generate flows with a non-negligible component of extensional deformation and where the onset of various elastic instabilities are observed. It was shown that these flows exhibit different types of flow transitions depending on geometry, *We* and *Re*, including: transition from a steady symmetric to a steady asymmetric flow, often followed by a second transition to unsteady flow at high *We*; direct transition between steady symmetric and unsteady flows. Moreover, the difference between Deborah and Weissenberg number also emphasized. In shear flows, viscoelastic fluids are also subject to shear-driven normal stresses and the ratio between the normal and shear stresses quantifies the non-linear response of the viscoelastic fluid and is proportional to the Weissenberg number. Furthermore, it was mentioned that elastic instabilities have both advantages and drawbacks in practical terms. When the objective is micro-mixing or high rates of heat and mass transfer, these low Reynolds number chaotic-like flows of elastic fluids provide a useful solution which is not available if the fluids are Newtonian (a similar situation here would require higher Reynolds numbers for chaotic advection to emerge). To conclude, it was concluded that the Weissenberg number in microchannels were ultimately responsible for the appearance of elastic instabilities at low or even negligible Reynolds numbers. They made a prediction that the popularity of micro flow systems requires the miniaturization of flow forcing methods and the use of electric and magnetic forcing mechanisms would become more common as an alternative to pressure driven flow.

Siginer and Letelier [14] investigated the inertial as well as elastic effects in the laminar flow of a class of non-affine viscoelastic fluids on the heat transfer behavior in pressure gradient driven laminar flow in straight tubes of non-circular shape and under constant temperature wall conditions. The temperature field were presented and discussed for several non-circular contours such as the ellipse and the equilateral triangle together with heat transfer behavior in terms of the Nusselt number. It is known that viscoelastic fluid flows at low Weissenberg number develop a steady secondary flow before the onset of a purely elastic instability. To show the effect of viscoelastic fluid flows on the heat transfer enhancement, they used the sufficiently low Weissenberg number. In addition, it was mentioned that heat transfer enhancement due to shear-thinning is identified together with the enhancement due to the inherent elasticity of the fluid which is the result of secondary flows in the cross-section. However, it is observed

that shear-thinning yields negligible heat transfer enhancement effect by comparing with the secondary flow effect [16]. Moreover, their simulations started with the thermal field at Newtonian fluids which is a consequence of velocity field at Newtonian fluid. While viscoelastic effects appeared, the longitudinal field was affected by the viscoelastic nature of the fluid, by both shear-thinning and first normal stress effects, and as a consequence the thermal field was altered separately with additive superposed effects by shear-thinning and elasticity. The longitudinal field was further changed with the secondary flow with a corresponding change in the thermal field, but more importantly a secondary flow triggered by unbalanced second normal stresses brought large changes to the temperature distribution and heat dissipation. As a result of their study, heat transfer due to shear-thinning was identified as well as the heat transfer enhancement due to secondary flows. Also, increasingly large enhancements could be computed with increasing elasticity of the fluid as compared to its Newtonian counterpart. It was said that large enhancements were possible even with dilute fluids. In addition to this paper, the physics of the interaction of the effects of the elasticity, viscoelastic Mach, Reynolds and Weissenberg numbers on generating the heat transfer enhancement is discussed in another study of Siginer and Letelier [15].

Naccache and Souza Mendes [16] investigated not only which parameters affect the secondary flow intensity and heat transfer but also the flow of non-Newtonian fluids inside rectangular ducts. The flow was assumed to be fully developed laminar, incompressible and steady. The viscoelastic behavior of the flowing fluid was described via the Criminale-Ericksen-Filbery (CEF) constitutive equation. As shown in all articles, it was observed in this paper that heat transfer phenomena involving non-Newtonian fluids are significantly different from their Newtonian counterparts for laminar flows through ducts of noncircular cross sections. Both the viscosity dependence on shear rate (shear-thinning or shear-thickening) and secondary flows caused by elastic effects are two distinct effects causing these differences. Moreover, it is known that secondary flows are caused by elastic forces related to the second normal stress difference. It was mentioned that aspect ratio, Reynolds number, and the first normal stress difference influenced secondary flow in addition to second normal difference. However, the second normal stress difference plays the dominant role. As a result of their study, it was found that heat transfer was strongly enhanced by secondary flows, Nusselt numbers reaching values as large as three times those for

corresponding Newtonian ones. Also, it was observed that shear-thinning yielded negligible heat transfer enhancement effect, when compared with the secondary flow effect. In addition, maximum heat transfer was shown to occur for some combinations of parameters. Thus, it can be say that there are optimal aspect ratios and Reynolds numbers in the sense of maximum heat transfer, which depend on the fluid's mechanical behavior.

The influences of the second normal stress coefficient, the Reynolds number and the aspect ratio on the magnitude of the secondary flow were examined in the study of Gao and Hartnett [17]. This paper included a numerical study for the secondary flow of a Reiner-Rivlin non-Newtonian fluid in laminar flow through ducts of square and rectangular cross section. One of the results of this study indicated that the secondary flow had no significant effect on the streamwise velocity. Another result was concluded that the values of friction factor for a Reiner-Rivlin fluid increased slightly with Reynolds number and the dimensionless second normal stress coefficient. Thus, the secondary flows arising in a Reiner-Rivlin non-Newtonian fluid through a rectangular duct have a negligible effect on the friction factor. In addition, it was emphasized that the sign of the second normal stress difference depends on the viscosity, elasticity, and local velocity gradients. The magnitude of secondary flow also increases as Reynolds number increases. It was indicated that the magnitude of the secondary flow is dominated by dimensionless secondary flow coefficient (elastic behavior) and is also affected by Reynolds number (viscous behavior).

Gao and Hartnett [18] reported a numerical study for the fully developed heat transfer behavior of elastic non-Newtonian fluids in steady laminar flow through rectangular ducts. The influence of the second normal stress coefficient, Reynolds number, Peclet number and aspect ratio on the heat transfer was considered in their study. In addition, it was mentioned that the fully developed laminar flow in a circular pipe the influence of the non-Newtonian viscosity may be seen, but no influence of elastic behavior even for a viscoelastic fluid appears. On the contrary, in the case of non-circular channels these influences become more important, especially for viscoelastic fluids. For laminar flow of Newtonian and purely viscous non-Newtonian fluids through non-circular channels of constant cross-section there exists a main flow velocity with no secondary motions. However, in the case of viscoelastic fluids the normal stresses give rise to secondary motions. In addition, as comparing the heat transfer results

in the form of Nusselt number as a function of the second normal stress coefficient; they pointed out that the Nusselt number increases significantly as the second normal stress coefficient increases. These results demonstrate that the secondary flow, which is a result of the second normal stress difference, has a major effect on the heat transfer for non-Newtonian viscoelastic fluids in laminar flow through non-circular ducts. Therefore, the stronger secondary flow the higher value of the heat transfer is achieved. Moreover, as comparing the Nusselt numbers as a function of aspect ratio with constant Peclet number they concluded that the heat transfer increases as the aspect ratio increases due to the secondary flow. However, the influence of aspect ratio is complicated because the change of geometry affects both the distribution and the magnitude of secondary flow. It was found that the secondary flow, which is associated with the presence of second normal stresses, results in a significant increase in the heat transfer, especially for aspect ratios of 0.5 and 1.0.

Syrjala [19] investigated the fully developed laminar flow of non-Newtonian viscoelastic fluids in straight duct of rectangular cross-section with heat transfer by means of the finite element method. The viscoelastic behavior of the fluid was described using the Criminale-Ericksen-Fibley (CEF) constitutive relationship. The results were presented and discussed in terms of the secondary flow field, temperature field, friction factor and Nusselt number. First, it was emphasized that the strength of the secondary flow is mainly determined by the second normal stress coefficient which has an important influence on both the secondary flow and heat transfer. In this study, it was observed that an obvious consequence of the secondary flow is that the hotter fluid from the near wall region is effectively conveyed towards the center of the duct. Therefore, a significant heat transfer enhancement as a result of the secondary flow was computed for all duct aspect ratios, 1.0, 0.5 and 0.2, considered in the analysis. Next, the numerical simulations demonstrated that although the secondary flow arising from the elasticity of the fluid is relatively very weak as compared to the main flow in the streamwise direction, it may substantially enhance heat transfer with all duct aspect ratios. The heat transfer enhancement was particularly outstanding in the cases of high Prandtl number. In contrast, the friction factor, and hence the pressure drop, was essentially unaffected by the secondary flow. Finally, the Nusselt numbers were essentially higher in the flow cases involving a secondary flow than in the rectilinear flow case by comparing the temperature contours.

Chang and co-workers [20] performed a numerical study on the heat transfer mechanism of Newtonian and non-Newtonian fluids in 2 : 1 horizontal rectangular ducts. The effects of temperature dependence of viscosity, shear-thinning, buoyancy-induced secondary flow and secondary flow due to normal stress difference were contemplated to model the laminar flow and heat transfer behavior for Newtonian and non-Newtonian fluids. The three key findings were presented. The first findings is that for Newtonian fluid, Nusselt number decreases at first and then gradually increases due to the effect of buoyancy-induced secondary flow while for the case of both upper and lower walls heated. The second finding is that for non-Newtonian fluid, the effects of temperature dependence and shear-thinning on viscosity significantly influence the heat transfer mechanism. And the heat transfer enhancement is caused mainly by the axial velocity distortion. By a comparison of numerical results of Nusselt number, it is found that with stronger velocity distortion, there is a stronger heat transfer enhancement. The last finding is that the effect of buoyancy-induced secondary flow is much weaker in the case for non-Newtonian than that shown in the case for Newtonian. At the central zone of duct, the temperature and shear rate of fluid are all relatively lower and then the viscosity is relatively higher than that of near wall region. In addition to these findings, it is believed that the secondary flows caused by the normal stress differences may be the reason for the heat transfer enhancement in the fully developed region as reported by Gao and Hartnett [18].

It is known that creeping viscoelastic fluid flows through serpentine channels at low Weissenberg number develop a steady secondary flow [12] before the onset of a purely elastic instability. Beyond this linear instability the flow becomes increasingly complex, and develops elastic turbulence. Therefore, Whalley et al. [21] used the sufficiently high Weissenberg number to achieve a fully elastic turbulence regime. They demonstrated the potential of using elastic turbulence to enhance heat transfer in micro scale serpentine channel consisted of 20 half-loops with a square cross section. In their study, at very low flow rates, which *We* number was less than 5, the pressure drop and Nusselt number were essentially the same as the Newtonian values. Beyond this Weissenberg number up to 25 the purely elastic instability led to an increase in the pressure drop but the Nusselt number was only marginally affected. Beyond a Weissenberg number of 25, significant increases in normalized Nusselt number were observed. In their experimental investigation they showed that elastic

turbulence enhanced the heat transfer at the micro scale in their geometry by up to 300 percent with highest Weissenberg number ($We \approx 80$) under creeping flow conditions in comparison to that achieved by the equivalent Newtonian fluid flow.

3. ANALYSIS AND MODELLING

In the following sub sections conservation of mass, momentum, energy equations and the constitutive equation for Oldroyd-B [33] model for the incompressible flows of a non-Newtonian fluid are given. The integral forms of these equations are also shown. Then, the three-dimensional numerical discretization along *x*-, *y*- and *z*- directions is performed over the dual control volume. In this study, the flow is assumed to be periodic in the streamwise and spanwise direction so that periodic boundary conditions can be employed at the inflow and outflow boundaries. This enables simulations that are relatively inexpensive with respect to both required computer memory and time. Therefore, the equations of boundary conditions applied in this study are given and their discretizations are also shown.

The present numerical method is based on the side-centered finite volume method on unstructured hexahedral meshes as described in Sahin [34]. That method is presented for parallel large-scale solution of the viscoelastic fluid flows with exact mass conservation within each element. In this approach, the velocity vector components and temperature are defined at the midpoint of each cell face, while the pressure term and the extra stress tensor are defined at element centroids. The present arrangement of the primitive variables leads to a stable numerical scheme and it does not require any *ad-hoc* modifications in order to enhance the pressure–velocity–stress coupling. The time stepping algorithm used decouples the calculation of the polymeric stress by solution of a hyperbolic constitutive equation from the evolution of the velocity and pressure fields by solution of a generalized Stokes problem. The energy equation is discretized by using the same discretization used in the momentum equation. Therefore, the temperature variables are also defined at the midpoint of each cell face as in the velocity variables. The resulting algebraic linear systems are solved using the FGMRES(m) Krylov iterative method with the restricted additive Schwarz preconditioner for the extra stress tensor and energy equation and the geometric non-nested multilevel preconditioner for the Stokes system. The computer program used in this study was written in Fortran. All the computations were performed with

96 Intel(R) Xeon(R) CPU E5 – 2690 cores with 2.90 GHz at TUBITAK ULAKBIM, High Performance and Grid Computing Center. The solutions of the each time step last approximately 80 seconds. The implementation of the preconditioned Krylov subspace algorithm, matrix-matrix multiplication and the multilevel preconditioner were carried out using the PETSc (Portable, Extensible Toolkit for Scientific Computation) software package [35] developed at the Argonne National Laboratories. The computational domain is decomposed into a set of sub-domains or partitions using the METIS library [36].

3.1 Flow Equations in Cartesian Coordinate Systems

Conservation of mass, momentum and energy equations are valid for any coordinate system. In order to write them for a Cartesian coordinate system first we need to define the velocity vector components in these systems;

$$\mathbf{V} = u\mathbf{i} + v\mathbf{j} + w\mathbf{k} \tag{3.1}$$

The non-dimensional governing equations for the incompressible Oldroyd-B fluid flow in the Cartesian coordinate system can be written in dimensionless form as follows: the continuity equation

$$-\frac{\partial u}{\partial x} - \frac{\partial v}{\partial y} - \frac{\partial w}{\partial z} = 0 \tag{3.2}$$

the momentum equations

$$\begin{aligned} &Re\left[\frac{\partial u}{\partial t} + u\frac{\partial u}{\partial x} + v\frac{\partial u}{\partial y} + w\frac{\partial u}{\partial z}\right] = \\ &-\frac{\partial p}{\partial x} + \beta\left(\frac{\partial^2 u}{\partial x^2} + \frac{\partial^2 u}{\partial y^2} + \frac{\partial^2 u}{\partial z^2}\right) + \frac{\partial T_{xx}}{\partial x} + \frac{\partial T_{xy}}{\partial y} + \frac{\partial T_{xz}}{\partial z} \end{aligned} \tag{3.3}$$

$$\begin{aligned} &Re\left[\frac{\partial v}{\partial t} + u\frac{\partial v}{\partial x} + v\frac{\partial v}{\partial y} + w\frac{\partial v}{\partial z}\right] = \\ &-\frac{\partial p}{\partial y} + \beta\left(\frac{\partial^2 v}{\partial x^2} + \frac{\partial^2 v}{\partial y^2} + \frac{\partial^2 v}{\partial z^2}\right) + \frac{\partial T_{xy}}{\partial x} + \frac{\partial T_{yy}}{\partial y} + \frac{\partial T_{yz}}{\partial z} \end{aligned} \tag{3.4}$$

$$\begin{aligned} &Re\left[\frac{\partial w}{\partial t} + u\frac{\partial w}{\partial x} + v\frac{\partial w}{\partial y} + w\frac{\partial w}{\partial z}\right] = \\ &-\frac{\partial p}{\partial z} + \beta\left(\frac{\partial^2 w}{\partial x^2} + \frac{\partial^2 w}{\partial y^2} + \frac{\partial^2 w}{\partial z^2}\right) + \frac{\partial T_{xz}}{\partial x} + \frac{\partial T_{yz}}{\partial y} + \frac{\partial T_{zz}}{\partial z} \end{aligned} \tag{3.5}$$

the constitutive equation for Oldroyd-B model

$$\begin{aligned} &We\left[\frac{\partial T_{xx}}{\partial t} + u\frac{\partial T_{xx}}{\partial x} + v\frac{\partial T_{xx}}{\partial y} + w\frac{\partial T_{xx}}{\partial z}\right] - We\left[\frac{\partial u}{\partial x}T_{xx} + \frac{\partial u}{\partial y}T_{xy} + \frac{\partial u}{\partial z}T_{xz}\right] \\ &-We\left[\frac{\partial u}{\partial x}T_{xx} + \frac{\partial u}{\partial y}T_{xy} + \frac{\partial u}{\partial z}T_{xz}\right] = (1-\beta)\left(\frac{\partial u}{\partial x} + \frac{\partial u}{\partial x}\right) - T_{xx} \end{aligned} \tag{3.6}$$

$$We\left[\frac{\partial T_{yy}}{\partial t}+u\frac{\partial T_{yy}}{\partial x}+v\frac{\partial T_{yy}}{\partial y}+w\frac{\partial T_{yy}}{\partial z}\right]-We\left[\frac{\partial v}{\partial x}T_{xy}+\frac{\partial v}{\partial y}T_{yy}+\frac{\partial v}{\partial z}T_{yz}\right]$$
$$-We\left[\frac{\partial v}{\partial x}T_{xy}+\frac{\partial v}{\partial y}T_{yy}+\frac{\partial v}{\partial z}T_{yz}\right]=(1-\beta)\left(\frac{\partial v}{\partial y}+\frac{\partial v}{\partial y}\right)-T_{yy} \quad \textbf{(3.7)}$$

$$We\left[\frac{\partial T_{zz}}{\partial t}+u\frac{\partial T_{zz}}{\partial x}+v\frac{\partial T_{zz}}{\partial y}+w\frac{\partial T_{zz}}{\partial z}\right]-We\left[\frac{\partial w}{\partial x}T_{xz}+\frac{\partial w}{\partial y}T_{yz}+\frac{\partial w}{\partial z}T_{zz}\right]$$
$$-We\left[\frac{\partial w}{\partial x}T_{xz}+\frac{\partial w}{\partial y}T_{yz}+\frac{\partial w}{\partial z}T_{zz}\right]=(1-\beta)\left(\frac{\partial w}{\partial z}+\frac{\partial w}{\partial z}\right)-T_{zz} \quad \textbf{(3.8)}$$

$$We\left[\frac{\partial T_{xy}}{\partial t}+u\frac{\partial T_{xy}}{\partial x}+v\frac{\partial T_{xy}}{\partial y}+w\frac{\partial T_{xy}}{\partial z}\right]-We\left[\frac{\partial u}{\partial x}T_{xy}+\frac{\partial u}{\partial y}T_{yy}+\frac{\partial u}{\partial z}T_{yz}\right]$$
$$-We\left[\frac{\partial v}{\partial x}T_{xx}+\frac{\partial v}{\partial y}T_{xy}+\frac{\partial v}{\partial z}T_{xz}\right]=(1-\beta)\left(\frac{\partial u}{\partial y}+\frac{\partial v}{\partial x}\right)-T_{xy} \quad \textbf{(3.9)}$$

$$We\left[\frac{\partial T_{xz}}{\partial t}+u\frac{\partial T_{xz}}{\partial x}+v\frac{\partial T_{xz}}{\partial y}+w\frac{\partial T_{xz}}{\partial z}\right]-We\left[\frac{\partial u}{\partial x}T_{xz}+\frac{\partial u}{\partial y}T_{yz}+\frac{\partial u}{\partial z}T_{zz}\right]$$
$$-We\left[\frac{\partial w}{\partial x}T_{xx}+\frac{\partial w}{\partial y}T_{xy}+\frac{\partial w}{\partial z}T_{xz}\right]=(1-\beta)\left(\frac{\partial u}{\partial z}+\frac{\partial w}{\partial x}\right)-T_{xz} \quad \textbf{(3.10)}$$

$$We\left[\frac{\partial T_{yz}}{\partial t}+u\frac{\partial T_{yz}}{\partial x}+v\frac{\partial T_{yz}}{\partial y}+w\frac{\partial T_{yz}}{\partial z}\right]-We\left[\frac{\partial v}{\partial x}T_{xz}+\frac{\partial v}{\partial y}T_{yz}+\frac{\partial v}{\partial z}T_{zz}\right]$$
$$-We\left[\frac{\partial w}{\partial x}T_{xy}+\frac{\partial w}{\partial y}T_{yy}+\frac{\partial w}{\partial z}T_{yz}\right]=(1-\beta)\left(\frac{\partial v}{\partial z}+\frac{\partial w}{\partial y}\right)-T_{yz} \quad \textbf{(3.11)}$$

the energy equation

$$\left[\frac{\partial \theta}{\partial t}+u\frac{\partial \theta}{\partial x}+v\frac{\partial \theta}{\partial y}+w\frac{\partial \theta}{\partial z}\right] = \frac{1}{RePr}\left[\frac{\partial^2\theta}{\partial x^2}+\frac{\partial^2\theta}{\partial y^2}+\frac{\partial^2\theta}{\partial z^2}\right] \quad \textbf{(3.12)}$$

where u, v and w are the velocity components in the x-, y- and z- directions, respectively, p is the pressure, $\boldsymbol{T}$ is the extra stress tensor and θ is the temperature. The dimensionless parameters are the Reynolds number $Re = R\langle U\rangle/\upsilon$, the Weissenberg number $We = \lambda\langle U\rangle/R$, the viscosity ratio β and the Prandtl number $Pr = \upsilon/\alpha$ where R is the channel minimum radius, U is the average velocity at inlet, λ is the relaxation time, υ is the kinematic viscosity and α is the thermal diffusion rate of the fluid. Reynolds number is seen in the momentum and energy equations. In the energy equation we also have Prandtl numbers. The Reynolds number is defined as the ratio of inertial forces to viscous forces and consequently quantifies the relative importance of these two types of forces for given flow conditions. High and low *Re* flows are said to be inertial force dominated and viscous force dominated, respectively. Prandtl number is the ratio of momentum and thermal diffusivities. As it gets larger the importance of diffusion term on the right hand side diminishes and the convective heat transfer modeled by the terms on the left hand side becomes more dominant. Multiplication

of Reynolds and Prandtl numbers is called the Peclet number (*Pe*). It is defined to be the ratio of the rate of advection to the rate of diffusion. The *We* number is used in the study of viscoelastic flows. The dimensionless number is the ratio of the relaxation time of the fluid and a specific process time. For instance, in simple steady shear, the *We* number is defined as the shear rate ($\dot{\gamma}$) times the relaxation time (λ).

3.2 Mathematical and Numerical Formulation

The governing equations for the incompressible Oldroyd-B fluid flow in the Cartesian coordinate system can be written in dimensionless form as follows: the continuity equation

$$-\nabla \cdot \mathbf{u} = 0 \tag{3.13}$$

the momentum equations

$$Re\left[\frac{\partial \mathbf{u}}{\partial t} + (\mathbf{u}\cdot\nabla)\mathbf{u}\right] + \nabla P = \beta\nabla^2\mathbf{u} + \nabla\cdot\mathbf{T} \tag{3.14}$$

the constitutive equation for Oldroyd-B model

$$We\left[\frac{\partial \mathbf{T}}{\partial t} + (\mathbf{u}\cdot\nabla)\mathbf{T} - (\nabla\mathbf{u})^T\cdot\mathbf{T} - \mathbf{T}\cdot\nabla\mathbf{u}\right] = (1-\beta)(\nabla\mathbf{u} + \nabla\mathbf{u}^T) - \mathbf{T} \tag{3.15}$$

the energy equation

$$RePr\left[\frac{\partial \theta}{\partial t} + (\mathbf{u}\cdot\nabla)\theta\right] = \nabla^2\theta \tag{3.16}$$

In these equations **u** represents the velocity vector, P is the pressure, **T** is the extra stress tensor and θ is the temperature. The dimensionless parameters are the Reynolds number *Re*, the Weissenberg number *We*, the viscosity ratio β which is equal to 1 for Newtonian fluids and the Prandtl number *Pr*. It is known that the Peclet number *Pe* is equivalent to the product of the Reynolds number and the Prandtl number.

The integral form of the continuity and constitutive equations over an unstructured hexahedral element Ω_e with boundary $\partial\Omega_e$ can be written in the Cartesian coordinates system in dimensionless form as follows: the continuity equation

$$-\oiint_{\partial\Omega_e} \mathbf{n}\cdot\mathbf{u}\,dS = 0 \tag{3.17}$$

the constitutive equation for Oldroyd-B model

$$\begin{aligned} &We\left[\iiint_{\Omega_e}\left(\frac{\partial \mathbf{T}}{\partial t}-(\nabla \mathbf{u})^T\cdot\mathbf{T}-\mathbf{T}\cdot\nabla\mathbf{u}\right)dV+\oiint_{\partial\Omega_e}(\mathbf{n}\cdot\mathbf{u})\mathbf{T}dS\right] \\ &=(1-\beta)\oiint_{\partial\Omega_e}(\mathbf{un}+\mathbf{nu})dS-\iiint_{\Omega_e}\mathbf{T}dV \end{aligned} \tag{3.18}$$

The integral form of the momentum and energy equation over an arbitrary dual control volume Ω_d with boundary $\partial\Omega_d$ can be written in the Cartesian coordinates system in dimensionless form as follows,

$$\begin{aligned} &Re\iiint_{\Omega_d}\frac{\partial \mathbf{u}}{\partial t}dV+Re\oiint_{\partial\Omega_d}(\mathbf{n}\cdot\mathbf{u})\mathbf{u}dS+\oiint_{\partial\Omega_d}\mathbf{n}pdS \\ &=\beta\oiint_{\partial\Omega_d}\mathbf{n}\cdot\nabla\mathbf{u}dS+\oiint_{\partial\Omega_d}\mathbf{n}\cdot\mathbf{T}dS \end{aligned} \tag{3.19}$$

the energy equation

$$RePr\iiint_{\Omega_d}\frac{\partial\theta}{\partial t}dV+RePr\oiint_{\partial\Omega_d}(\mathbf{n}\cdot\mathbf{u})\theta dS=\oiint_{\partial\Omega_d}\mathbf{n}\cdot\nabla\theta dS \tag{3.20}$$

In these equations, V is the control volume and S is the control volume surface area, $\mathbf{n}$ represents the outward normal vector. The above governing equations are discretized using the side-centered finite volume method on unstructured hexahedral meshes. Figure 3.1 illustrates two neighboring three-dimensional hexahedral elements with an arbitrary dual control volume constructed by connecting the element centroids to the common vertices shared by the both hexahedral elements. The velocity vector components and temperature are defined at the mid-point of each cell face while the pressure and the extra stress tensor are defined at the element centroids.

3.2.1 Three-Dimensional numerical discretization

The numerical method is based on the side-centered finite volume method on unstructured hexahedral meshes as described in [34]. The momentum equations along the *x*-, *y*- and *z*- directions are discretized over the dual control volume shown in Figure 3.1 and the discretization volume involves only the right and left elements that share the common face where the components of the velocity vector are discretized. The discrete contribution from the right cell shown in Figure 3.1 is given below for each

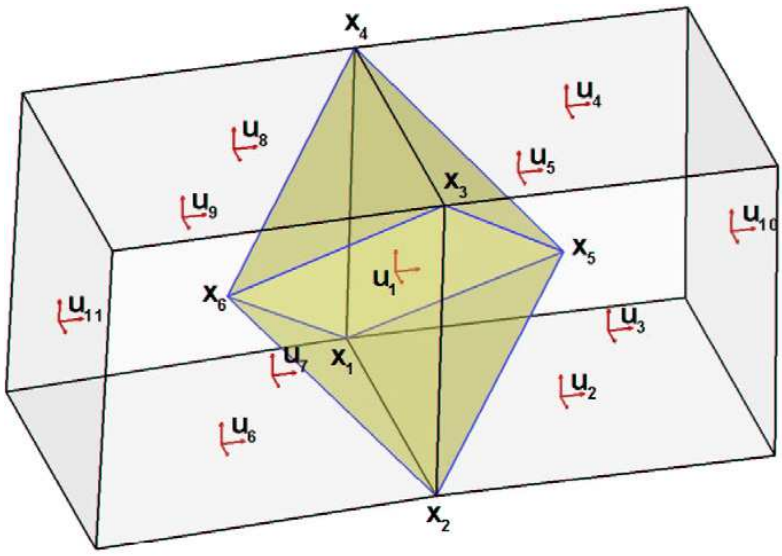

Figure 3.1: Three-dimensional unstructured mesh with a dual control volume.

term of the momentum equation along *x*- direction.

The time derivative

$$Re\left[\frac{3u_1^{n+1}}{4\Delta t}+\frac{\sum_i u_i^{n+1}}{6\cdot 4\Delta t}\right]V_{12345}-Re\left[\frac{3u_1^{n}}{4\Delta t}+\frac{\sum_i u_i^{n}}{6\cdot 4\Delta t}\right]V_{12345} \qquad \textbf{(3.21)}$$
$$with \quad i=1,2,3,4,5,10$$

The convective term

$$\begin{aligned} &Re[\mathbf{u}_{125}^{n}\cdot\mathbf{A}_{125}]u_{125}^{n+1}+Re[\mathbf{u}_{235}^{n}\cdot\mathbf{A}_{235}]u_{235}^{n+1} \\ &Re[\mathbf{u}_{345}^{n}\cdot\mathbf{A}_{345}]u_{345}^{n+1}+Re[\mathbf{u}_{415}^{n}\cdot\mathbf{A}_{415}]u_{415}^{n+1} \end{aligned} \qquad \textbf{(3.22)}$$

The viscous term

$$\begin{aligned} &-\beta\left[\left(\frac{\partial u}{\partial x}\right)_{125}^{n+1}\mathbf{A}_{125}\cdot\mathbf{i}+\left(\frac{\partial u}{\partial y}\right)_{125}^{n+1}\mathbf{A}_{125}\cdot\mathbf{j}+\left(\frac{\partial u}{\partial z}\right)_{125}^{n+1}\mathbf{A}_{125}\cdot\mathbf{k}\right] \\ &-\beta\left[\left(\frac{\partial u}{\partial x}\right)_{235}^{n+1}\mathbf{A}_{235}\cdot\mathbf{i}+\left(\frac{\partial u}{\partial y}\right)_{235}^{n+1}\mathbf{A}_{235}\cdot\mathbf{j}+\left(\frac{\partial u}{\partial z}\right)_{235}^{n+1}\mathbf{A}_{235}\cdot\mathbf{k}\right] \\ &-\beta\left[\left(\frac{\partial u}{\partial x}\right)_{345}^{n+1}\mathbf{A}_{345}\cdot\mathbf{i}+\left(\frac{\partial u}{\partial y}\right)_{345}^{n+1}\mathbf{A}_{345}\cdot\mathbf{j}+\left(\frac{\partial u}{\partial z}\right)_{345}^{n+1}\mathbf{A}_{345}\cdot\mathbf{k}\right] \\ &-\beta\left[\left(\frac{\partial u}{\partial x}\right)_{415}^{n+1}\mathbf{A}_{415}\cdot\mathbf{i}+\left(\frac{\partial u}{\partial y}\right)_{415}^{n+1}\mathbf{A}_{415}\cdot\mathbf{j}+\left(\frac{\partial u}{\partial z}\right)_{415}^{n+1}\mathbf{A}_{415}\cdot\mathbf{k}\right] \end{aligned} \qquad \textbf{(3.23)}$$

The extra stress term

$$\begin{aligned} &-\left[(T_{xx})_{125}^{n+1}\mathbf{A}_{125}\cdot\mathbf{i}+(T_{xy})_{125}^{n+1}\mathbf{A}_{125}\cdot\mathbf{j}+(T_{xz})_{125}^{n+1}\mathbf{A}_{125}\cdot\mathbf{k}\right] \\ &-\left[(T_{xx})_{235}^{n+1}\mathbf{A}_{235}\cdot\mathbf{i}+(T_{xy})_{235}^{n+1}\mathbf{A}_{235}\cdot\mathbf{j}+(T_{xz})_{235}^{n+1}\mathbf{A}_{235}\cdot\mathbf{k}\right] \\ &-\left[(T_{xx})_{345}^{n+1}\mathbf{A}_{345}\cdot\mathbf{i}+(T_{xy})_{345}^{n+1}\mathbf{A}_{345}\cdot\mathbf{j}+(T_{xz})_{345}^{n+1}\mathbf{A}_{345}\cdot\mathbf{k}\right] \\ &-\left[(T_{xx})_{415}^{n+1}\mathbf{A}_{415}\cdot\mathbf{i}+(T_{xy})_{415}^{n+1}\mathbf{A}_{415}\cdot\mathbf{j}+(T_{xz})_{415}^{n+1}\mathbf{A}_{415}\cdot\mathbf{k}\right] \end{aligned} \qquad \textbf{(3.24)}$$

The pressure term

$$\begin{aligned}&\left[\frac{p_1+p_2+p_5}{3}\right]^{n+1}\mathbf{A}_{125}\cdot\mathbf{i}+\left[\frac{p_2+p_3+p_5}{3}\right]^{n+1}\mathbf{A}_{235}\cdot\mathbf{i}\\&\left[\frac{p_3+p_4+p_5}{3}\right]^{n+1}\mathbf{A}_{345}\cdot\mathbf{i}+\left[\frac{p_4+p_1+p_5}{3}\right]^{n+1}\mathbf{A}_{415}\cdot\mathbf{i}\end{aligned} \tag{3.25}$$

where V_{12345} is the volume of the pyramid between the points $\mathbf{x}_1$, $\mathbf{x}_2$, $\mathbf{x}_3$, $\mathbf{x}_4$ and $\mathbf{x}_5$ shown in Figure 3.1, Δt is the time step, $\mathbf{A}_{125}$, $\mathbf{A}_{235}$, $\mathbf{A}_{345}$ and $\mathbf{A}_{415}$ are the area vectors of the dual volume triangular surfaces. The area vectors are computed from the cross product of vectors (as an example, $\mathbf{A}_{125}=0.5(\mathbf{x}_2-\mathbf{x}_5)(\mathbf{x}_1-\mathbf{x}_5)$. The values $\mathbf{u}_{125}$, $\mathbf{u}_{235}$, $\mathbf{u}_{345}$ and $\mathbf{u}_{415}$ are the velocity vectors defined at the mid-point of each dual volume triangular surfaces and p_1, p_2, p_3, p_4 and p_5 are the pressure values at the points $\mathbf{x}_1$, $\mathbf{x}_2$, $\mathbf{x}_3$, $\mathbf{x}_4$ and $\mathbf{x}_5$, respectively.

The discretization of the momentum equation along the *y*- and *z*- direction follows very closely the ideas presented here. The continuity equation (3.17) is integrated within each hexahedral elements Ω_e and evaluated using the mid-point rule on each of the element faces.

$$-\sum_{j=1}^{6}\left[[u^{n+1}A_x]_j+[v^{n+1}A_y]_j+[w^{n+1}A_z]_j\right]=0 \tag{3.26}$$

where $\mathbf{A}=A_x\mathbf{i}+A_y\mathbf{j}+A_z\mathbf{k}$ is the hexahedral element surface area vector and u, v and w are the velocity vector components defined at the mid-point of each hexahedral element face. The constitutive equation for the Oldroyd-B fluid is discretized as in Sahin and Wilson [37] within each hexahedral element Ω_e assuming that the extra stresses $\mathbf{T}_i$ and velocity gradients $\nabla\mathbf{u}_i$ are constant:

$$\begin{aligned}&We\left[\frac{\mathbf{T}_i^{n+1}-\mathbf{T}_i^n}{\Delta t}V_e-(\nabla\mathbf{u}_i^n)^\top\cdot\mathbf{T}_i^{n+1}V_e-\mathbf{T}_i^{n+1}\cdot\nabla\mathbf{u}_i^nV_e\right]\\&+\left[\sum_{j=1}^{6}\left[[u^nA_x]_j+[v^nA_y]_j+[w^nA_z]_j\right]\mathbf{T}_j^{n+1}\right]\\&=(1-\beta)\left[\nabla\mathbf{u}_i^{n+1}+(\nabla\mathbf{u}_i^{n+1})^\top\right]V_e-\mathbf{T}_i^{n+1}V_e\end{aligned} \tag{3.27}$$

Where V_e is the volume of the hexahedral element, A_e is the hexahedral element surface area vector and T_j is the value of the extra stress tensor defined at the element centroids. In order to extrapolate the extra stresses to the boundaries of the finite volume elements the second-order upwind least square interpolation described above is used in order to maintain stability for hyperbolic constitutive equations. The time-dependent finite

volume discretization of the above equations leads to a linear system of equations of the form:

$$\begin{bmatrix} A_{\tau\tau} & A_{\tau u} & 0 \\ A_{u\tau} & A_{uu} & A_{up} \\ 0 & A_{pu} & 0 \end{bmatrix} \begin{bmatrix} \tau \\ u \\ p \end{bmatrix} = \begin{bmatrix} b_1 \\ b_2 \\ 0 \end{bmatrix} \tag{3.28}$$

The above linear system of algebraic equations should be solved for each time step. It should be noted that the discretization of above equations leads to a saddle point problem.

The heat equation is one way coupled from those equations. Therefore, the heat equations are discretized over the dual control volume shown in Figure 3.1 and the discretization volume involves only the right and left elements that share the common face where the components of the temperature are discretized. The discrete contribution from the right cell shown in Figure 3.1 is given below for each term of the energy equation.

The time derivative

$$Pe\left[\frac{3\theta_1^{n+1}}{4\Delta t}+\frac{\sum_i \theta_i^{n+1}}{6\cdot 4\Delta t}\right]V_{12345} - Pe\left[\frac{3\theta_1^{n}}{4\Delta t}+\frac{\sum_i \theta_i^{n}}{6\cdot 4\Delta t}\right]V_{12345} \qquad with \quad i=1,2,3,4,5,10 \tag{3.29}$$

The advection (convection) term

$$\begin{aligned} &Pe[\mathbf{u}_{125}^n\cdot\mathbf{A}_{125}]\theta_{125}^{n+1} + Pe[\mathbf{u}_{235}^n\cdot\mathbf{A}_{235}]\theta_{235}^{n+1} \\ &Pe[\mathbf{u}_{345}^n\cdot\mathbf{A}_{345}]\theta_{345}^{n+1} + Pe[\mathbf{u}_{415}^n\cdot\mathbf{A}_{415}]\theta_{415}^{n+1} \end{aligned} \tag{3.30}$$

The diffusion term

$$\begin{aligned} &-\left[\left(\frac{\partial\theta}{\partial x}\right)_{125}^{n+1}\mathbf{A}_{125}\cdot\mathbf{i}+\left(\frac{\partial\theta}{\partial y}\right)_{125}^{n+1}\mathbf{A}_{125}\cdot\mathbf{j}+\left(\frac{\partial\theta}{\partial z}\right)_{125}^{n+1}\mathbf{A}_{125}\cdot\mathbf{k}\right] \\ &-\left[\left(\frac{\partial\theta}{\partial x}\right)_{235}^{n+1}\mathbf{A}_{235}\cdot\mathbf{i}+\left(\frac{\partial\theta}{\partial y}\right)_{235}^{n+1}\mathbf{A}_{235}\cdot\mathbf{j}+\left(\frac{\partial\theta}{\partial z}\right)_{235}^{n+1}\mathbf{A}_{235}\cdot\mathbf{k}\right] \\ &-\left[\left(\frac{\partial\theta}{\partial x}\right)_{345}^{n+1}\mathbf{A}_{345}\cdot\mathbf{i}+\left(\frac{\partial\theta}{\partial y}\right)_{345}^{n+1}\mathbf{A}_{345}\cdot\mathbf{j}+\left(\frac{\partial\theta}{\partial z}\right)_{345}^{n+1}\mathbf{A}_{345}\cdot\mathbf{k}\right] \\ &-\left[\left(\frac{\partial\theta}{\partial x}\right)_{415}^{n+1}\mathbf{A}_{415}\cdot\mathbf{i}+\left(\frac{\partial\theta}{\partial y}\right)_{415}^{n+1}\mathbf{A}_{415}\cdot\mathbf{j}+\left(\frac{\partial\theta}{\partial z}\right)_{415}^{n+1}\mathbf{A}_{415}\cdot\mathbf{k}\right] \end{aligned} \tag{3.31}$$

where V_{12345} is the volume of the pyramid between the points $\mathbf{x}_1$, $\mathbf{x}_2$, $\mathbf{x}_3$, $\mathbf{x}_4$ and $\mathbf{x}_5$ shown in Figure 3.1, Δt is the time step, $\mathbf{A}_{125}$, $\mathbf{A}_{235}$, $\mathbf{A}_{345}$ and $\mathbf{A}_{415}$ are the area vectors of the dual volume triangular surfaces. The values $\mathbf{u}_{125}$, $\mathbf{u}_{235}$, $\mathbf{u}_{345}$ and $\mathbf{u}_{415}$ are the velocity vectors defined at the mid-point of each dual volume triangular surfaces. Also,

the values θ_{125}, θ_{235}, θ_{345} and θ_{415} are the temperature defined at the mid-point of each dual volume triangular surfaces. However, the temperature values are known at the mid-point of the element faces and the temperature values at $\mathbf{x}_1$, $\mathbf{x}_2$, $\mathbf{x}_3$, and $\mathbf{x}_4$ have to be computed. To compute the temperature at $\mathbf{x}_1$, as an example, a second-order Taylor series expansion can be written as

$$\theta_i = \theta_i + \frac{\partial \theta}{\partial x}|_{x=x_1}\left(x_{f,i} - x_1\right) + \frac{\partial \theta}{\partial y}|_{x=x_1}\left(y_{f,i} - y_1\right) + \frac{\partial \theta}{\partial z}|_{x=x_1}\left(z_{f,i} - z_1\right) \qquad \textbf{(3.32)}$$
$$with \quad i = 1, 2, [...], l$$

where l represent the number of the faces connected to the point $\mathbf{x}_1$ and $\mathbf{x}_{f,i}$ corresponds to the face mid-points. This overdetermined system of linear equations may be solved in a least square sense using the normal equation approach, in which both sides are multiplied by the transpose. The modified system is solved using the singular value decomposition provided by LAPACK driver in order to avoid the numerical difficulties associated with solving linear systems with near rank deficiency. In a similar manner, the u, v, w velocity vector components and pressure values at $\mathbf{x}_1$, $\mathbf{x}_2$, $\mathbf{x}_3$, and $\mathbf{x}_4$ are computed using the same approach.

The temperature values θ_{125}, θ_{235}, θ_{345} and θ_{415} are computed at the mid-point of the dual volume triangular surfaces using the least square interpolations. As an example,

$$\theta_{125} = \beta\left[\theta_1 + \nabla\theta_1 \mathbf{r}_1\right] + (1-\beta)\left[\theta_2 + \nabla\theta_2 \mathbf{r}_2\right] \qquad \textbf{(3.33)}$$

where β is a weight factor determining the type of convection scheme used, $\nabla\theta_1$ and $\nabla\theta_2$ are the gradients of temperature where the θ_1 and θ_2 temperature values are defined and $\mathbf{r}_1$ and $\mathbf{r}_2$ are the distance vectors from the mid-point of the dual volume triangular surfaces to the locations where the gradients of temperature are computed, i.e. $\mathbf{r}_1 = (\mathbf{x}_{125} - \mathbf{x}_{f,1})$ and $\mathbf{r}_2 = (\mathbf{x}_{125} - \mathbf{x}_{f,2})$ with $\mathbf{x}_{125} = (\mathbf{x}_1 + \mathbf{x}_2 + \mathbf{x}_5)/3$. In this study, we will employ only $\beta = 0.5$ which corresponds to the central least square interpolation. For evaluating the gradient terms, $\nabla\theta_1$ and $\nabla\theta_2$, a least square procedure is used in which the temperature data is assumed to behave linearly. Referring to Figure 3.1 as an example, the following system can be constructed for the term $\nabla\theta_1$

$$\begin{bmatrix} x_{f,2}-x_{f,1} & y_{f,2}-y_{f,1} & z_{f,2}-z_{f,1} \\ x_{f,3}-x_{f,1} & y_{f,3}-y_{f,1} & z_{f,3}-z_{f,1} \\ x_{f,4}-x_{f,1} & y_{f,4}-y_{f,1} & z_{f,4}-z_{f,1} \\ x_{f,5}-x_{f,1} & y_{f,5}-y_{f,1} & z_{f,5}-z_{f,1} \\ x_{f,6}-x_{f,1} & y_{f,6}-y_{f,1} & z_{f,6}-z_{f,1} \\ x_{f,7}-x_{f,1} & y_{f,7}-y_{f,1} & z_{f,7}-z_{f,1} \\ x_{f,8}-x_{f,1} & y_{f,8}-y_{f,1} & z_{f,8}-z_{f,1} \\ x_{f,9}-x_{f,1} & y_{f,9}-y_{f,1} & z_{f,9}-z_{f,1} \end{bmatrix} \begin{bmatrix} \frac{\partial\theta}{\partial x} \\ \frac{\partial\theta}{\partial y} \\ \frac{\partial\theta}{\partial z} \end{bmatrix} = \begin{bmatrix} \theta_2-\theta_1 \\ \theta_3-\theta_1 \\ \theta_4-\theta_1 \\ \theta_5-\theta_1 \\ \theta_6-\theta_1 \\ \theta_7-\theta_1 \\ \theta_8-\theta_1 \\ \theta_9-\theta_1 \end{bmatrix} \tag{3.34}$$

This overdetermined system of linear equations may be solved for $\nabla\theta_1$ in a least square sense using the same normal equation approach. The gradient term $\nabla\theta_2$ is computed in a similar manner.

The temperature gradients defined at the mid-point of each dual volume triangular faces can be computed using the Green-Gauss theorem:

$$\nabla\theta = \frac{\partial\theta}{\partial x}\mathbf{i} + \frac{\partial\theta}{\partial y}\mathbf{j} + \frac{\partial\theta}{\partial z}\mathbf{k} = \frac{1}{V_c}\oiint_{\partial\Omega_c}\theta d\mathbf{A} \tag{3.35}$$

where V_c covolume consists of two tetrahedral elements that share the same dual volume triangular surface area with their fourth vertices located at the midpoint of the hexahedral element faces. The right-hand side of the equation (3.35) is evaluated using the mid-point rule on each of the covolume faces. The contribution from the left cell is also calculated in a similar manner. In addition, the *u*, *v*, *w* velocity vector components and their gradients are computed using the same approach as shown above.

The time-dependent finite volume discretization of the energy equations leads to a linear system and it should be solved for each time step. The form of the linear system is given below;

$$[A_{\theta\theta}]\,[\theta] = [b_1] \tag{3.36}$$

3.2.2 Iterative solver

In practice, the solution of equation (3.28) does not converge very quickly and it is rather difficult to construct robust preconditioners for the whole coupled system because of the zero-block in the saddle point problem. Therefore, we decouple the system by using a time-splitting technique which decouples the calculation of extra stresses from the evaluation of the velocity and pressure fields by solving a generalized Navier-Stokes problem. The stress equation

$$[A_{\tau\tau}]\,[\tau] = [b_1 - uA_{\tau u} - vA_{\tau v} - wA_{\tau w}] \tag{3.37}$$

The Navier-Stokes problem

$$\begin{bmatrix} A_{uu} & 0 & 0 & A_{up} \\ 0 & A_{vv} & 0 & A_{vp} \\ 0 & 0 & A_{ww} & A_{wp} \\ A_{pu} & A_{pv} & A_{pw} & 0 \end{bmatrix} \begin{bmatrix} u \\ v \\ w \\ p \end{bmatrix} = \begin{bmatrix} b_2 - \tau A_{u\tau} \\ b_3 - \tau A_{v\tau} \\ b_4 - \tau A_{w\tau} \\ 0 \end{bmatrix} \tag{3.38}$$

In the present paper, we use an upper triangular right preconditioner which results in a scaled discrete Laplacian instead of a zero block in the original system. Then the modified system becomes

$$\begin{bmatrix} A_{uu} & 0 & 0 & A_{up} \\ 0 & A_{vv} & 0 & A_{vp} \\ 0 & 0 & A_{ww} & A_{wp} \\ A_{pu} & A_{pv} & A_{pw} & 0 \end{bmatrix} \begin{bmatrix} I & 0 & 0 & -A_{up} \\ 0 & I & 0 & -A_{vp} \\ 0 & 0 & I & -A_{wp} \\ 0 & 0 & 0 & I \end{bmatrix} \begin{bmatrix} q \\ r \\ s \\ p \end{bmatrix} = \begin{bmatrix} b_2 - \tau A_{u\tau} \\ b_3 - \tau A_{v\tau} \\ b_4 - \tau A_{w\tau} \\ 0 \end{bmatrix} \tag{3.39}$$

where

$$\begin{bmatrix} u \\ v \\ w \\ p \end{bmatrix} = \begin{bmatrix} I & 0 & 0 & -A_{up} \\ 0 & I & 0 & -A_{vp} \\ 0 & 0 & I & -A_{wp} \\ 0 & 0 & 0 & I \end{bmatrix} \begin{bmatrix} q \\ r \\ s \\ p \end{bmatrix} \tag{3.40}$$

and the zero block is replaced with $-A_{pu}A_{up} - A_{pv}A_{vp} - A_{pw}A_{wp}$ which is a scaled discrete Laplacian. Unfortunately, this leads to a significant increase in the number of non-zero elements due to the matrix–matrix multiplication. However, it is possible to replace the $-A_{pu}A_{up} - A_{pv}A_{vp} - A_{pw}A_{wp}$ block matrix in the upper triangular right preconditioner with a computationally less expensive matrix. The calculations indicate that the largest contribution for the pressure gradients in the momentum equations comes from the right and left elements that share the common face where the components of the velocity vector are discretized. Therefore, we will use the contribution from these two elements for the block matrix which leads maximum three non-zero entries per row. Although, this approximation does not change the convergence rate of an iterative solver significantly, it leads to a significant reduction in the computing time and memory requirement.

3.3 Boundary Conditions

The continuity and constitutive equation are discretized over the element. However, the momentum and energy equations are discretized over an arbitrary dual control volume as shown in Figure 3.1. Therefore, we must modify the momentum and energy equation or use boundary conditions on the boundary.

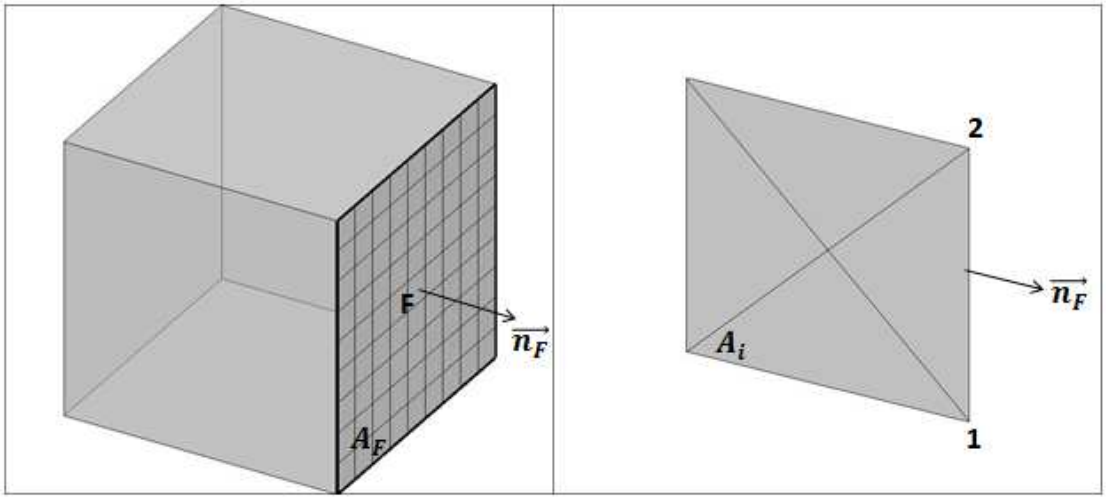

Figure 3.2: Element on the boundary.

3.3.1 Traction Free boundary condition

Momentum equation is modified over a boundary faces. Three and two dimensional element at the boundary is shown in Figure 3.2.

The momentum equation and its integral form are given below;

$$Re \iiint_{A_e} \frac{\partial \mathbf{u}}{\partial t} dV + Re \oiint_{A_F} (\mathbf{n} \cdot \mathbf{u}) \mathbf{u} dS + \oiint_{A_F} \mathbf{n} p dS = \oiint_{A_F} \mathbf{n} \cdot \nabla \mathbf{u} dS \quad \textbf{(3.41)}$$

The material derivation is neglected for outflow condition. Then,

$$\oiint_{A_F} \mathbf{n} p dS = \oiint_{A_F} \mathbf{n} \cdot \nabla \mathbf{u} dS \quad \textbf{(3.42)}$$

is performed on the A_F as shown in Figure 3.2. The gradient and pressure value at the point of F is accepted to be equal to the gradient and pressure value in the center point of the element. The velocity gradient at the point of F is calculated as follow;

$$\nabla u|_F = \frac{1}{V} \oiint_{V_e} u d\mathbf{A} \quad \textbf{(3.43)}$$

where $d\mathbf{A} = A_x \mathbf{i} + A_y \mathbf{j} + A_z \mathbf{k}$. Then,

$$p_F \, \mathbf{A}_F = \frac{1}{V} \, \mathbf{u} \sum_{j=1}^{6} \left[\mathbf{A}_j \cdot \mathbf{A}_F \right] \quad \textbf{(3.44)}$$

is performed on the A_F, where $\mathbf{A}_F = \mathbf{n} \cdot dS$ and V is the volume of the element.

The discretization of that equation along the x- direction is given below.

$$p\,(A_x)_F = \frac{1}{V}\sum_{j=1}^{6}\left[u^{n+1}A_x\right]_j (A_x)_F + \frac{1}{V}\sum_{j=1}^{6}\left[u^{n+1}A_y\right]_j (A_y)_F + \frac{1}{V}\sum_{j=1}^{6}\left[u^{n+1}A_z\right]_j (A_z)_F \tag{3.45}$$

The current application of the outflow boundary condition is compatible with the discretization of the incompressible Navier-Stokes equations.

3.3.2 Neumann boundary condition

For the case of Neumann boundary condition for fluid flow, the velocity gradient values are set to zero at boundary.

$$\frac{\partial u}{\partial n} = \mathbf{n}\cdot\nabla u \;=\; 0 \tag{3.46}$$

The integral form of that equation,

$$\mathbf{n}\cdot\frac{1}{V}\oiint_{V_e}\mathbf{u}d\mathbf{A} \;=\; 0 \tag{3.47}$$

where $\mathbf{n} = A_x\mathbf{i} + A_y\mathbf{j} + A_z\mathbf{k}$ is the normal vector at the faces of the element, $\mathbf{u}$ is the velocity vector.

$$\mathbf{n}\cdot\sum_{j=1}^{6}\left[[\mathbf{u}^{n+1}A_x]_j + [\mathbf{u}^{n+1}A_y]_j + [\mathbf{u}^{n+1}A_z]_j\right] \;=\; 0 \tag{3.48}$$

The discretization of that equation along the x- direction is given below. The discretization along the y- and z- direction follows the same way.

$$\sum_{j=1}^{6}\left[n_x[u^{n+1}A_x]_j + n_y[u^{n+1}A_y]_j + n_z[u^{n+1}A_z]_j\right] \;=\; 0 \tag{3.49}$$

For the case of constant heat flux at wall, the temperature gradient values are set to unity; whereas, for the case of insulated boundary condition at wall, the temperature gradient values are set to zero. For constant heat flux

$$\frac{\partial u}{\partial n} = \mathbf{n}\cdot\nabla\theta = 1 \tag{3.50}$$

where,

$$\nabla\theta = \frac{1}{V}\oiint_{\partial\Omega_e}\theta d\mathbf{A} = \frac{1}{V_e}\left[\oiint_{\partial\Omega_f}\theta A_x\mathbf{i} + \oiint_{\partial\Omega_f}\theta A_y\mathbf{j} + \oiint_{\partial\Omega_f}\theta A_z\mathbf{k}\right] \tag{3.51}$$

where $d\mathbf{A} = A_x\mathbf{i} + A_y\mathbf{j} + A_z\mathbf{k}$ is the normal vector at the faces of the element, θ is the temperature values, $\partial\Omega_f$ is the faces of the element. The discretization of the equation (3.50) is given below.

$$\frac{1}{V_e}\left[n_x \sum_{j=1}^{6} [\theta^{n+1}A_x]_j + n_y[\theta^{n+1}A_y]_j + n_z[\theta^{n+1}A_z]_j\right] = 1 \qquad \textbf{(3.52)}$$

where, $\mathbf{n} = n_x\mathbf{i} + n_y\mathbf{j} + n_z\mathbf{k}$ is the normal vector of the face at the boundary.

3.3.3 Periodic boundary condition

We studied the flow and temperature fields under the assumption of fully developed flow, which means that the flow pattern repeats itself from module to module. In such circumstances it is sufficient to analyze only one segment (module) of the geometry. Periodic flow and heat transfer occur widely in a variety of industrial applications. Fully developed periodic boundary conditions have been employed to effect performance calculations for heat and mass exchange devices. Numerical analyses of fully developed laminar flow and heat transfer in geometry that is periodically repetitive will be carried out with streamwise and spanwise periodicity in *x*- and *z*- directions. Constant wall temperature (Dirichlet) and constant heat flux (Neumann) boundary conditions may be considered in this study. These conditions have been examined by Rosaguti et al. [10], Murthy and Mathur [38], Beale [39], Patankar et al. [40], Kelkar and Patankar [41] and Niceno and Nobile [42]. Solution procedure for periodic flow and heat transfer are given below.

3.3.3.1 Flow periodicity

Consider a domain with periodic boundaries separated by a translation vector $\overrightarrow{\mathrm{L}}$, i.e. wavelength *L*, as shown in Figure 3.3. The two periodic boundaries of the domain are denoted as periodic and periodic shadow for convenience. This domain represents one of a series of periodic modules translated by $\overrightarrow{\mathrm{L}}$. They constitute counterpart of each other's. Therefore, we can employ side-center finite volume methods at the boundary faces [38]. If the flow is fully developed, the pressure field can be expressed as the linear combination of the local pressure and the overall pressure drop [39, 42]

$$u_{in} = u_{out} \qquad \textbf{(3.53)}$$

$$p_{in} = p_{out} + \Delta p \qquad \textbf{(3.54)}$$

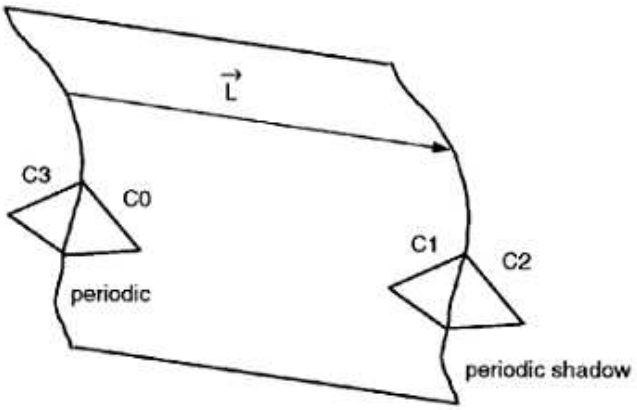

Figure 3.3: Periodic domain [38].

where the local component p repeats itself from module to module. A no-slip boundary condition for velocity is enforced on the walls of the channels, and a periodic boundary condition is applied at the inflow and outflow of the computational domain. The continuity and constitutive equation discretized over the each element. However, the momentum and energy equations are discretized over an arbitrary dual control volume shown in Figure 3.1 and the discretization volume involves only the right and left elements that share the common face where the components of the velocity vector and temperature are discretized. Periodic and periodic shadow elements can be used to create that dual control volume. In other words, C_1 is the left side of the C_0, contrary C_0 is the right side of the C_1 as shown in Figure 3.3. In addition to this, additional equations (3.54) must be added to the system of algebraic equations.

3.3.3.2 Temperature periodicity

For the temperature field, there are two fundamental types of boundary conditions which can be prescribed on the walls: constant heat flux ($H2$ boundary condition) or constant temperature (T boundary condition). The discretization at the boundaries are discussed below for these two cases. For the solution of the temperature field, a non-dimensional temperature is introduced (3.55).

$$\vartheta = \left(\frac{\overline{\mathrm{T_w}} - T_{x,y}}{\overline{\mathrm{T_w}} - \overline{\mathrm{T_B}}} \right) \qquad \textbf{(3.55)}$$

In the study of Beale [39], for constant heat flux, the temperature field is piecewise linear $T(0,y,z) = T(l,y,z) + c$, whereas for constant wall temperature the non-dimensional temperature ϑ is equal at both the inlet and the outlet where $\vartheta = (T - T_w)/(T_0 - T_w)$ and T_0 is a reference temperature, often chosen as the bulk value.

These may be combined to obtain [39];

$$T_{in} = c_1 T_{out} + c_2 \tag{3.56}$$

$$c_1 = \begin{cases} \frac{T_B|_{in} - T_w}{T_B|_{out} - T_w} & constant \quad T_w \\ 1 & constant \quad q_w \end{cases}$$

$$c_2 = \begin{cases} T_w(1-c_1) & constant \quad T_w \\ T_B|_{out} - T_B|_{in} & constant \quad q_w \end{cases}$$

According to another study of Rosaguti et al. [10], in order to simulate fully developed conditions, temperatures are scaled from the outlet of the serpentine unit to the inlet. Temperature fields are scaled to allow calculation of the fully developed temperature field by imposing the condition that the non-dimensional temperature is equal at both the inlet and the outlet of the repeating unit of interest [10]:

$$\vartheta_{in} = \left(\frac{\overline{\mathrm{T_w}} - T_{x,y}}{\overline{\mathrm{T_w}} - \overline{\mathrm{T_B}}} \right)_{in} = \left(\frac{\overline{\mathrm{T_w}} - T_{x,y}}{\overline{\mathrm{T_w}} - \overline{\mathrm{T_B}}} \right)_{out} = \vartheta_{out} \tag{3.57}$$

where

$$\overline{\mathrm{T_w}} = \frac{1}{P} \int_P T_w dp \tag{3.58}$$

is the perimeter-averaged wall temperature at an axial location s, and

$$\overline{\mathrm{T_B}} = \frac{1}{\dot{m} c_p} \int_{A_s} \rho u_s c_p T_{x,y} dA_s \tag{3.59}$$

is the bulk mean temperature at an axial location s, with $T_{x,y}$ being the temperature at location (x,y) in the section at s.

For the case of constant wall temperature (T boundary condition), T_w is constant, and the following form of equation (3.57) is used to determine the required inlet temperatures:

$$T_{x,y}|_{in} = T_w - \left(T_w - \overline{\mathrm{T_B}}|_{in}\right) \left(\frac{T_w - T_{x,y}|_{out}}{T_w - \overline{\mathrm{T_B}}|_{out}} \right) \tag{3.60}$$

where T_w and $\overline{\mathrm{T_B}}|_{in}$ in are specified and $\overline{\mathrm{T_B}}|_{out}$ is obtained from the simulation.

For the case of constant wall heat flux ($H2$ boundary condition), temperature profiles are identical in shape at the entrance and exit, but are displaced by an amount that is proportional to the wall heat flux and the wall area. The mean wall temperature, $\bar{T_w}$, in this case, varies along the axial path s. As temperature profiles are identical in shape

$$T_{x,y}|_{out} - T_{x,y}|_{in} = \Delta T_s \tag{3.61}$$

An overall heat balance gives

$$\overline{\mathrm{T_B}}|_{out} - \overline{\mathrm{T_B}}|_{in} = \frac{qA}{\dot{m}c_p} \tag{3.62}$$

So

$$\Delta T_s = \frac{qA}{\dot{m}c_p} \tag{3.63}$$

The desired inlet temperatures are determined from scaled outlet temperatures through the use of equations (3.60) and (3.61) for fully developed flow in the modules.

Same formulations are examined by Murthy and Mathur [38], Patankar et al. [40] and Kelkar and Patankar [41]. For constant heat flux boundary condition, time dependent constitutive and momentum equation are solved; therefore, the energy equations are also solved in each time step. Therefore; time dependent periodic boundary condition must be used. Those formulations give accurate heat dissipation with steady solution. However, the current velocity distribution is neither periodic nor steady due to viscoelastic instability. Thus, constant heat flux, $H2$, cannot be employ at the periodic faces, inlet and outlet.

The solutions of the energy equation (3.16) along with the boundary conditions (3.57) and (3.60) presents an eigenvalue problem, since it is the variable θ that behaves in a periodic fashion and since the T_B along streamwise direction is not known a priori. In other word, in the study of Murthy and Mathur [38], the solution of the energy equation (3.16) represents a non-linear problem for the constant temperature boundary condition. Murthy and Mathur [38] suggest to link the non-dimensional temperature field with the bulk temperature in an iterative fashion in each time step. Instead of this, Niceno and Nobile [42] offered to scale the temperature profile from the outlet of the domain and copy it to the inlet; therefore, the profile can be used for the new iteration of the linear solver for the energy equation. This can be expressed by

$$T^n = \left(\frac{T_B|_{in} - T_w}{T_B^{n-1}|_{out} - T_w} \right) \left(T^{n-1}|_{out} - T_w \right) + T_w \tag{3.64}$$

where,

$$T_B = \frac{\iint \mathbf{u} T \, d\mathbf{A}}{\iint \mathbf{u} d\mathbf{A}} \tag{3.65}$$

where $d\mathbf{A}$ is the area of the cross-section. One variable remains to be set, and that is the bulk temperature at the inflow $T_B|_{in}$. At the outflow, a standard Neumann boundary condition is used.

In this study,

- The periodic velocity boundary condition with a constant mass flow rate is imposed at the inflow and outflow (the pressure jump is computed).
- The periodic velocity boundary condition with zero pressure jump is imposed in the spanwise direction.
- No-slip boundary boundary condition is used on solid walls.
- The wall temperature is fixed to 0.
- The inlet bulk temperature is unity.
- The inflow temperature is rescaled from the temperature at the outflow.

$$\theta_{in} = \alpha \quad \theta_{out} \tag{3.66}$$

where

$$\alpha = \frac{\iint \mathbf{u}\theta \cdot \mathbf{n} dydz}{\iint \mathbf{u} \cdot \mathbf{n} dydz} \tag{3.67}$$

- At the outflow, a standard Neumann boundary condition is used for energy equation.

$$\frac{\partial \theta}{\partial n} = 0 \tag{3.68}$$

4. THE NUMERICAL RESULTS

In this section, the pressure drop and heat transfer characteristics of microchannel heat sink are numerically analyzed. The three-dimensional numerical simulations are carried out within a micro serpentine channel in order to quantify to the importance of the three-dimensional inertial and viscoelastic instabilities for heat transfer enhancement. In this study, the flow is assumed to be periodic in the streamwise, x- direction and spanwise, z- direction as shown in Figure 4.1 so that periodic boundary conditions can be employed at the inflow and outflow boundaries. This enables simulations that are relatively inexpensive with respect to both required computer memory and time. Therefore, numerical analyses of incompressible fully developed laminar flow of a viscoelastic fluid and heat transfer will be carried out with streamwise and spanwise periodicity.

The three-dimensional geometry of a micro serpentine channel is provided in Figure 4.1 along with all hexahedral computational mesh. The $2D$ fine mesh consists of $47,898$ nodes and $47,293$ elements. The $3D$ mesh is an extrusion in the spanwise direction of a $2D$ mesh. Therefore, the $3D$ fine mesh which is used for numerical simulation consists of $641,121$ nodes and $613,400$ hexahedral elements ($11764,000$ DOF).

Numerical analyses of incompressible fully developed laminar flow of a viscoelastic fluid and heat transfer in serpentine channel which is periodically repetitive in the streamwise and spanwise directions have been carried out using the side-centered finite volume method on unstructured hexahedral meshes. The conservation of mass, momentum and energy equations and the constitutive equation for Oldroyd-B model are performed. The energy equation is one way coupled from the conservation of mass, momentum and Oldroyd-B constitutive equations. The numerical code is written using Fortran computer programming language. This code first solves the constitutive equations to find the stress tensor. Then, it solves the continuity and Navier-Stokes equations that are coupled to find the unknown velocity and pressure distribution without knowing the temperature. We assume that fluid properties are not a function

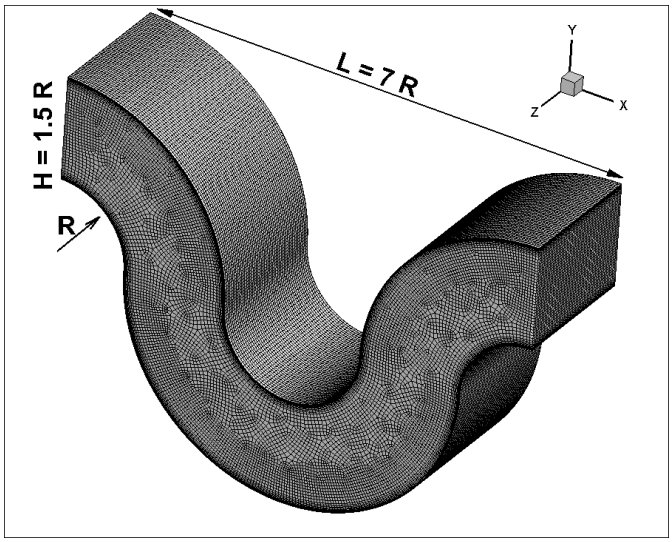

Figure 4.1: Geometric dimensions and 3D computational mesh for a serpentine channel with hexahedral elements.

of temperature. Having found the velocity field, heat equation can be solved to find the temperature distribution at each time step. All the computations were performed with 96 Intel(R) Xeon(R) CPU E5 – 2690 cores with 2.90 GHz at TUBITAK ULAKBIM, High Performance and Grid Computing Center. The solutions of the each time step last approximately 80 seconds. The non-dimensional numbers used in simulations are defined to be $We = \lambda\langle U\rangle/R$, $Re = R\langle U\rangle/\upsilon$ and $Pr = \upsilon/\alpha$ where R is the channel minimum radius, U is the average velocity at inlet, λ is the relaxation time, υ is the kinematic viscosity and α is the thermal diffusion rate of the fluid. The viscosity ratio β is set to 0.67. The boundary conditions are the no slip on the channel walls and spanwise and streamwise periodicity in z- and x- direction. At the inflow, the total mass flow rate is given and the periodic boundary condition with pressure jump is imposed. For energy equation we impose the bulk temperature at the inlet and the constant wall temperature is imposed on the solid walls. In the study, the velocity components are in the streamwise direction, x-, as u, in the wall normal or transverse direction, y-, as v, in the spanwise direction, z-, as w.

4.1 The Numerical Simulation of Flow Field

It is well known that viscoelastic fluid flows at low Weissenberg number develop a steady secondary flow before the onset of a purely elastic instability. However, beyond a critical Weissenberg number a time dependent purely elastic instability occurs. In addition, high Weissenberg number is ultimately responsible for the appearance of

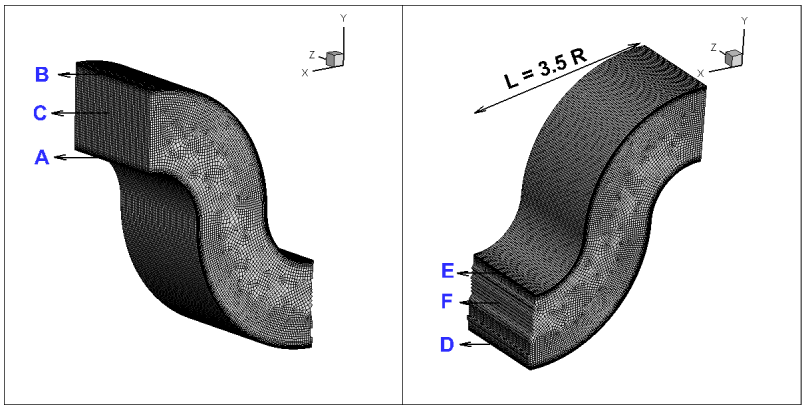

Figure 4.2: The sample nodes at inlet and middle of the channel both streamwise and spanwise direction.

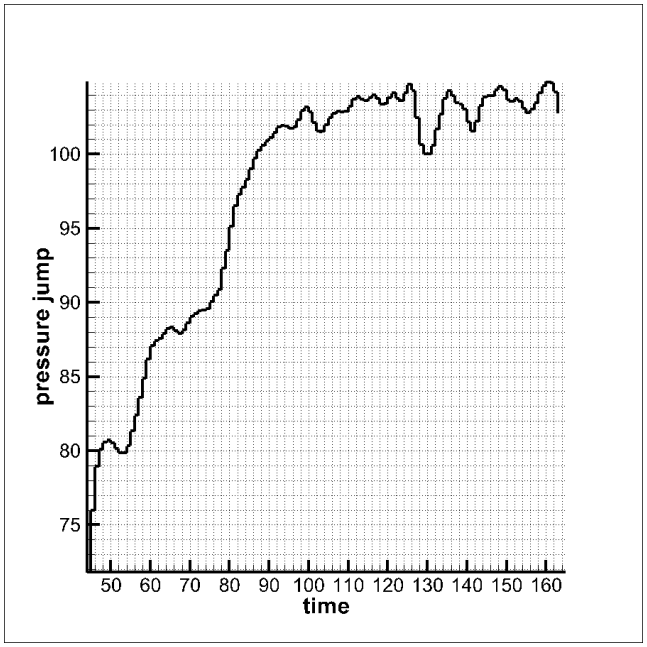

Figure 4.3: Pressure jump vs. time at $We = 8$ for $Re = 10$.

elastic instabilities at low or even negligible Reynolds numbers in microchannels [13]. The sample nodes are chosen in the channel to show the velocity and pressure jump values change over time as shown in Figure 4.2. These chosen nodes are at the inlet close to the middle of the channel both streamwise and spanwise directions. Figure 4.3 shows the pressure jump values changing over time from about 45 to 170 seconds. Therefore, the pressure jump or loss does not show a periodic or steady behavior.Time dependent constitutive and momentum equation are solved in each time step. The velocities at the monitoring locations show that the flow is unsteady as shown in Figure 4.4 and 4.5. Thus, the velocity distribution is neither periodic nor steady due to viscoelastic instability. However, for Newtonian fluid flow the velocity distribution is shown to be periodic in Figure 4.6.

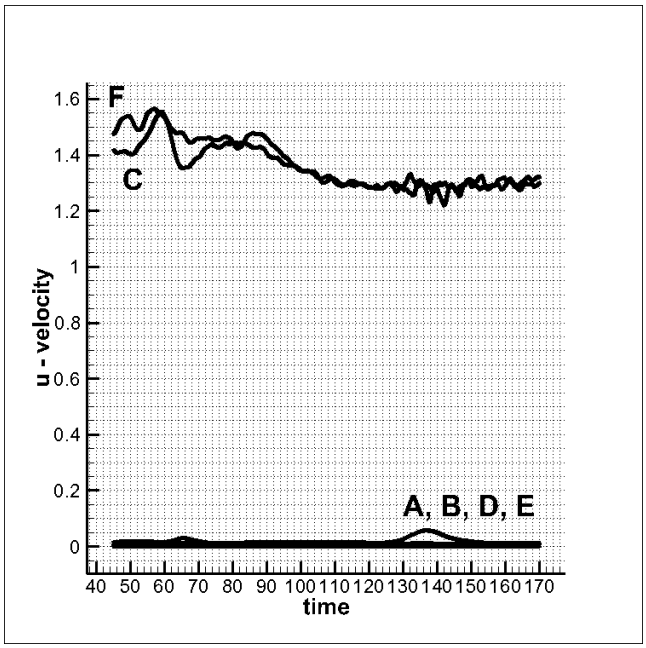

Figure 4.4: $u-$ velocity vs. time.

In this study, three-dimensional time dependent calculations are carried out beyond the first critical Weissenberg and Reynolds numbers in order to quantify the magnitude of the secondary vortices in the flow direction. The comparisons between Newtonian and non-Newtonian velocity component are shown in Figure 4.8. The simulations indicates that as the Reynolds number decreases, the strength of the spanwise vorticity component will be decreased and it will disappear completely below $Re = 50$. Also, streamwise vorticity component are compared in Figure 4.9. Therefore, it is not possible to use the inertial instabilities for the heat transfer enhancement. However, it is possible to use viscoelastic three-dimensional instabilities at lower Reynolds numbers by introducing a viscoelastic fluid as a coolant. Although it is clear that there will be there-dimensional instabilities beyond the critical Weissenberg number, the question is that how much heat transfer enhancement could be achievable by increasing the Weissenberg number. Therefore, the numerical simulations are performed at $Re = 10$ by increasing the Weissenberg number. The computed base flows are presented in Figure 4.6 at $We = 0$ and Figure 4.6 at $We = 8$. The comparison of the unsteady flow patterns illustrated experimentally by Galindo-Rosales et al. [13] and illustrated in this study with $We = 8$ is shown in Figure 4.7 to demonstrate the accuracy. From the comparison of the present simulations with the experimental result, we may say that the numerical simulations in the current study show a good agreement with the experimental results. In addition to that simulations, the development of the secondary

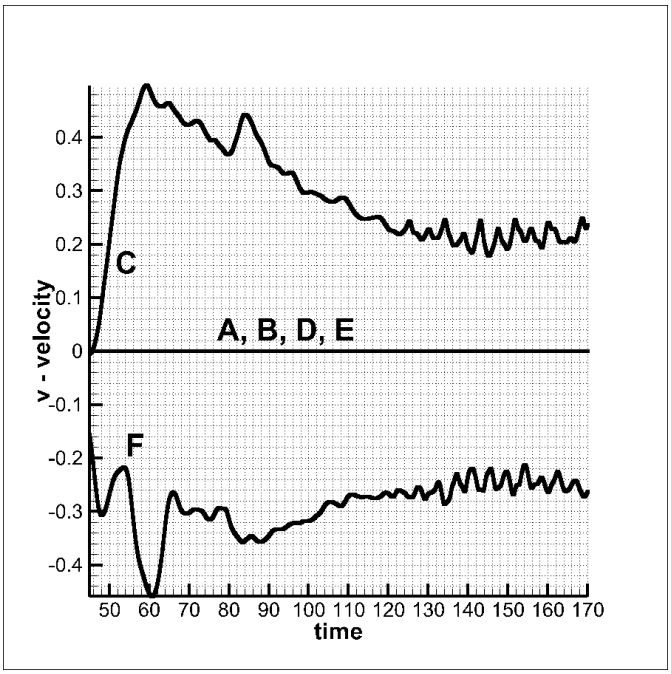

Figure 4.5: $v-$ velocity vs. time.

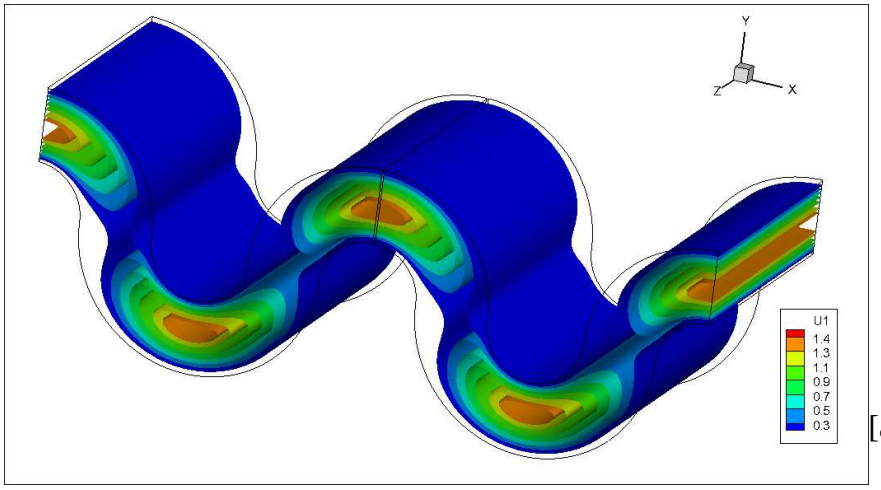

[a]

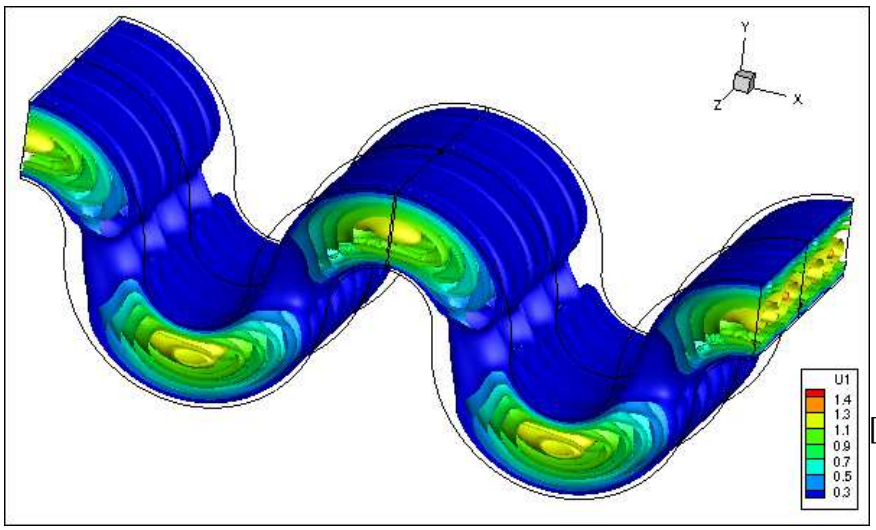

[b]

Figure 4.6: The comparison of the computed $u-$ velocity component at $We = 0$ for $Re = 10$ at $t = 20$ [a] and $We = 8$ for $Re = 10$ at $t = 170$ [b].

vortices due to viscoelastic instability are given Figure 4.10. Also, the components of the extra stress tensor are shown in Figure 4.11 at $t = 170$. It is well known that pressure drop is an important parameter for microchannel heat sink design. It leads to an increase in pumping power. It is intended that micro-cooling systems should be both thermally efficient and not expensive in terms of the pumping power. To evaluate efficiency, heat transfer enhancement and the pressure drop must be considered together. Therefore, pressure drop comparison is given in Figure 4.9.

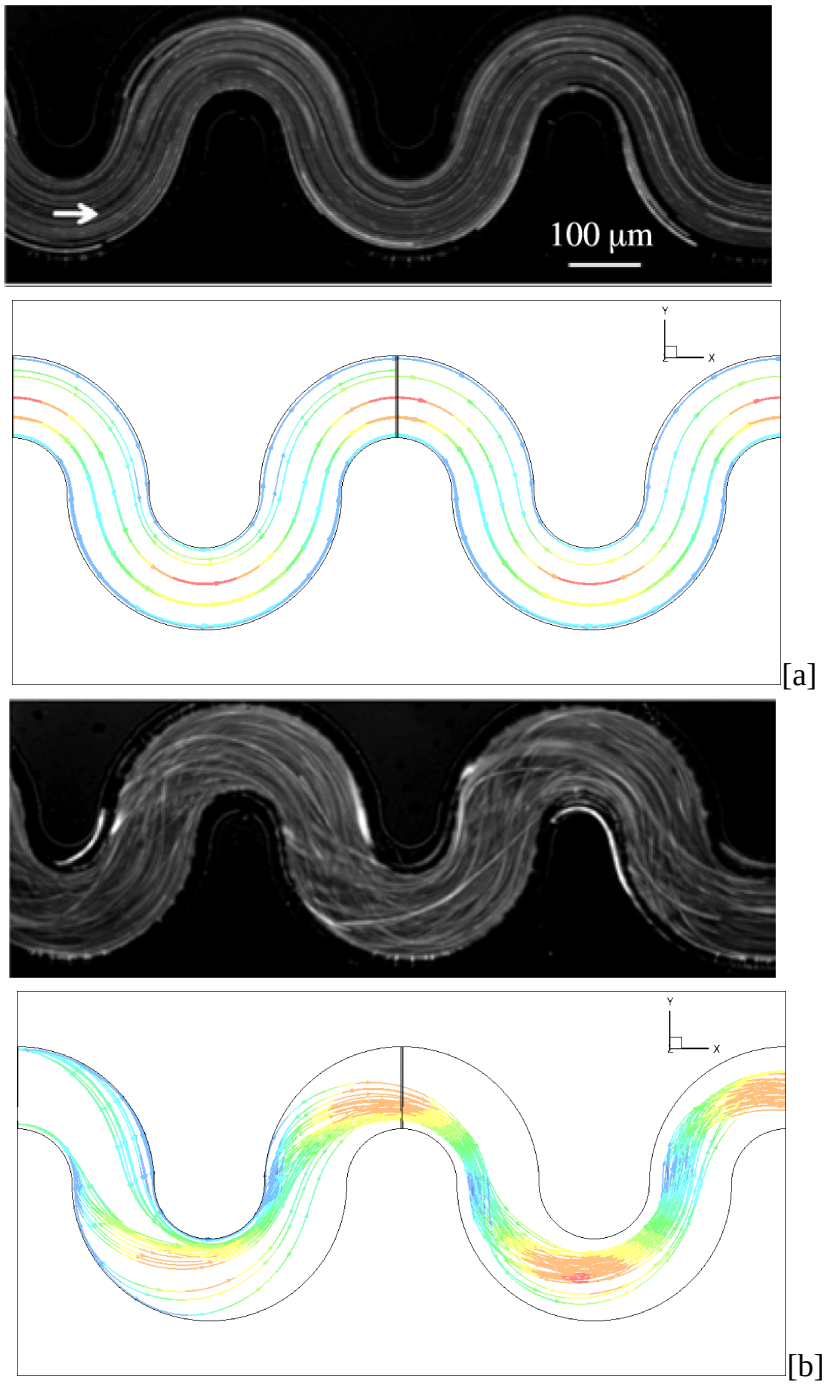

[a]

[b]

Figure 4.7: The comparison of the streamtrace for $We = 0$ at $t = 20$ with [13] [a] and $We = 8$ at $t = 170$[b].

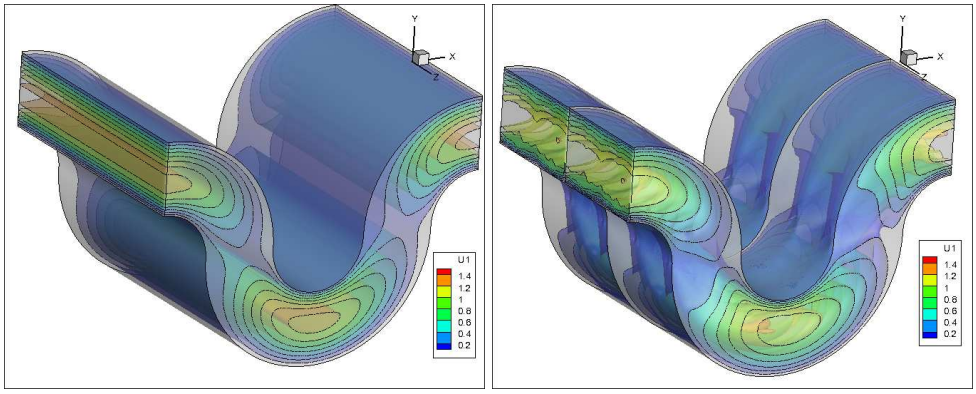

[a]

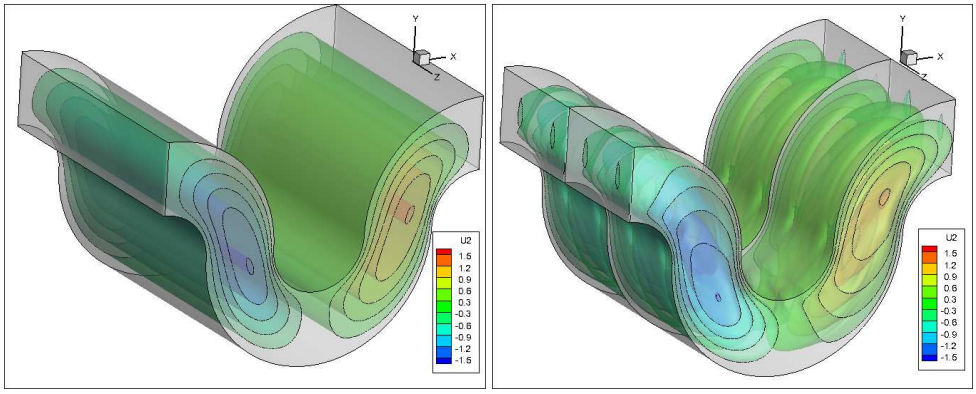

[b]

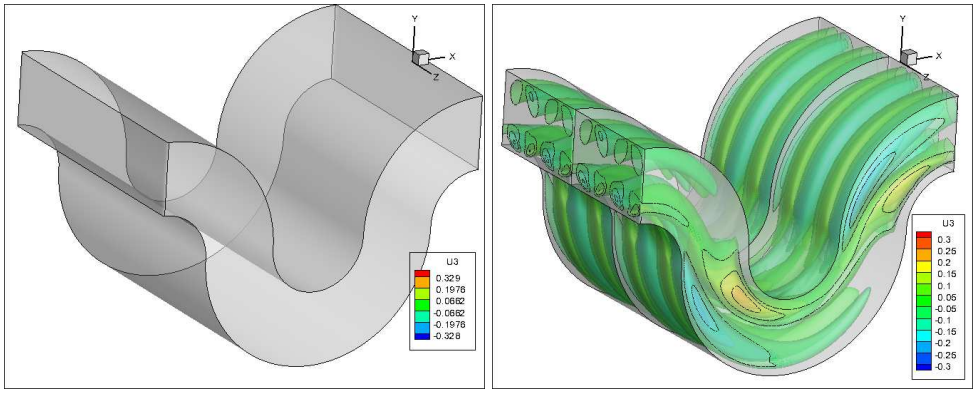

[c]

Figure 4.8: The comparison of the computed $u-$ [a], $v-$ [b] and $w-$ [c] velocity component for $We = 0$ at $t = 20$ (left) and $We = 8$ at $t = 170$ (right).

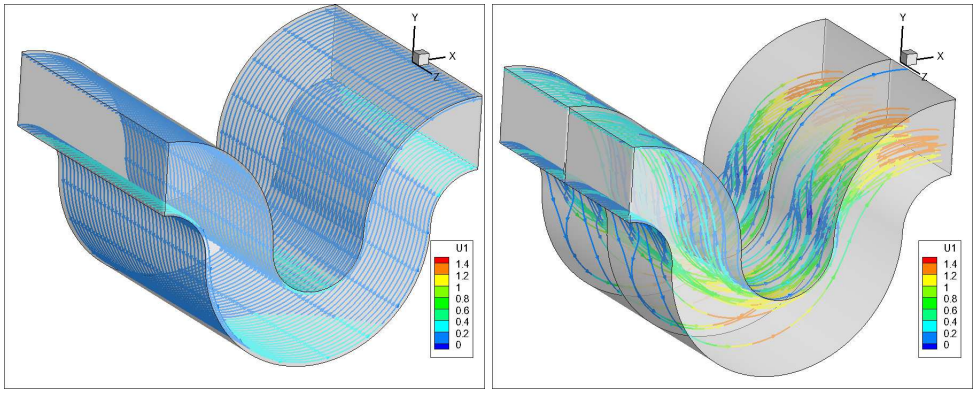

[a]

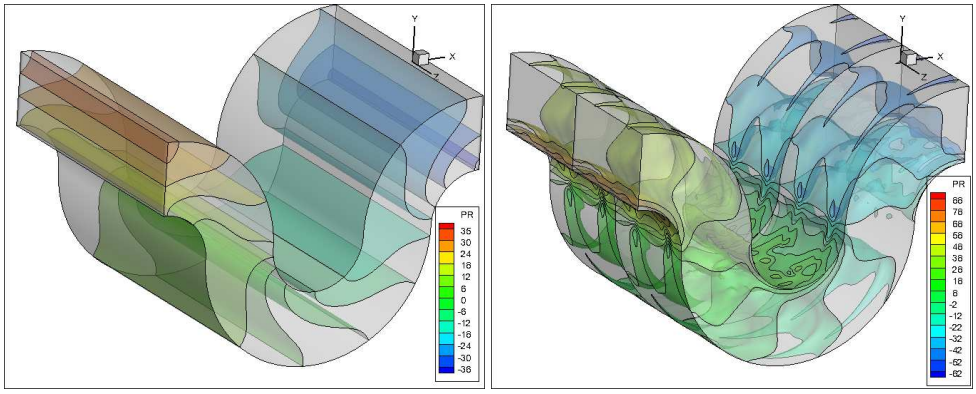

[b]

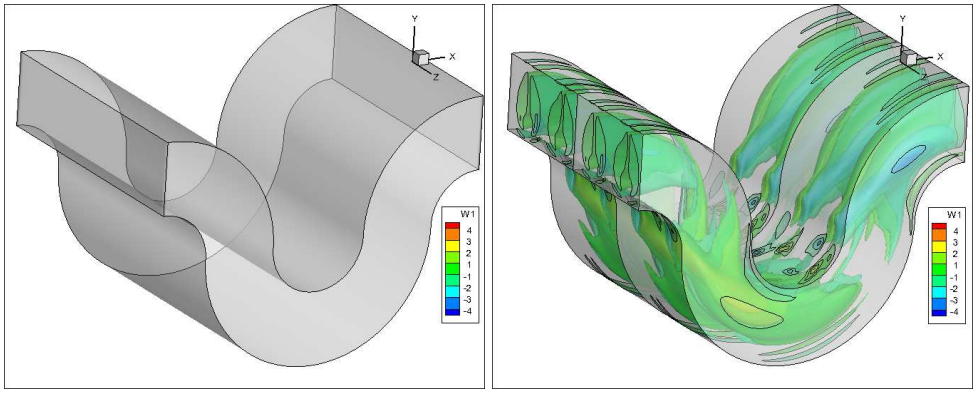

[c]

Figure 4.9: The comparison of the streamwise [a], pressure [b] and $x-$ vorticity [c] for $We = 0$ at $t = 20$ (left) and $We = 8$ at $t = 170$ (right).

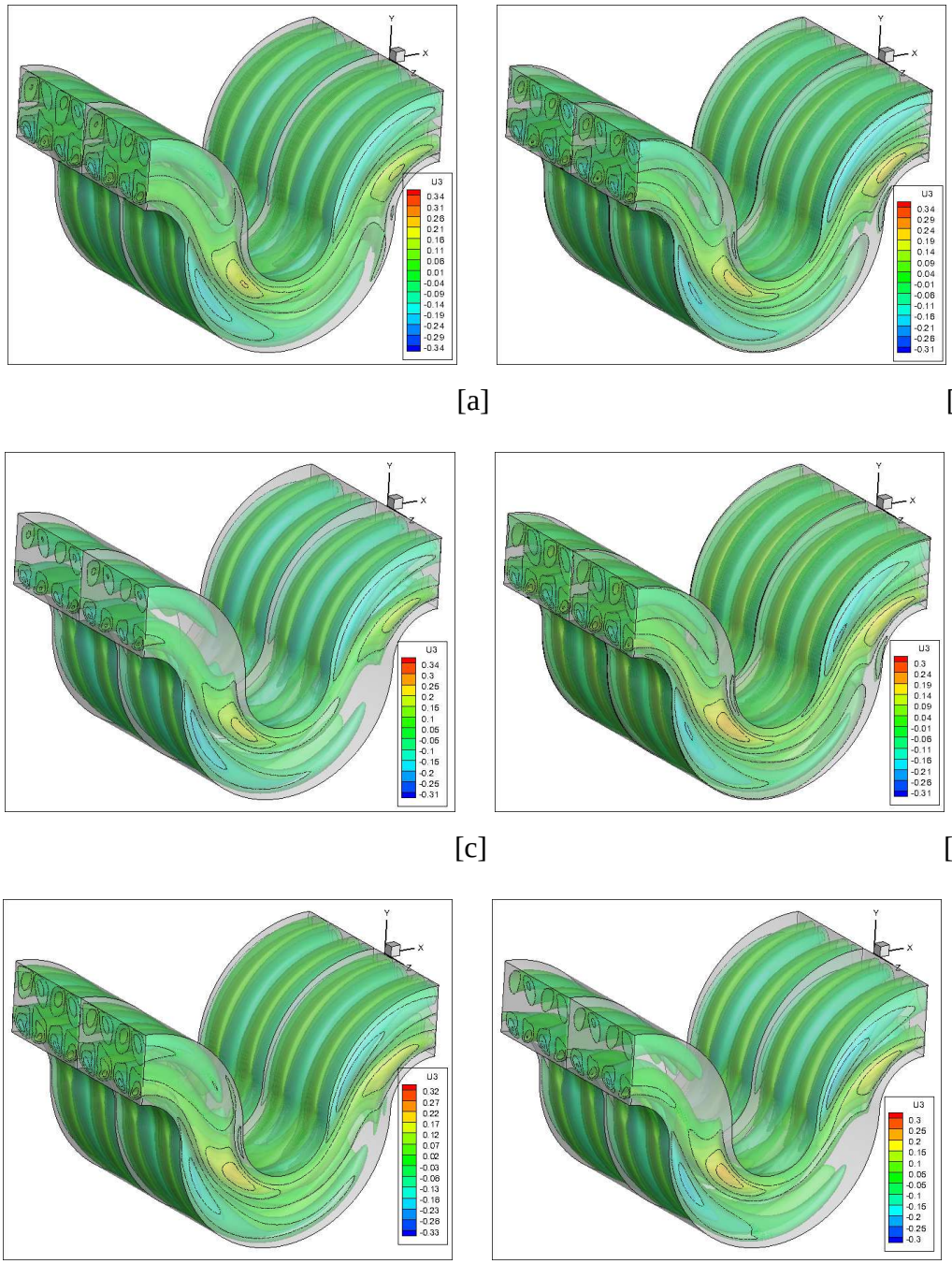

Figure 4.10: The snapshot of the spanwise velocity component for $We = 8$ and $Re = 10$ at $t = 145$ [a], $t = 150$ [b], $t = 155$ [c], $t = 160$ [d], $t = 165$ [e], $t = 170$ [f].

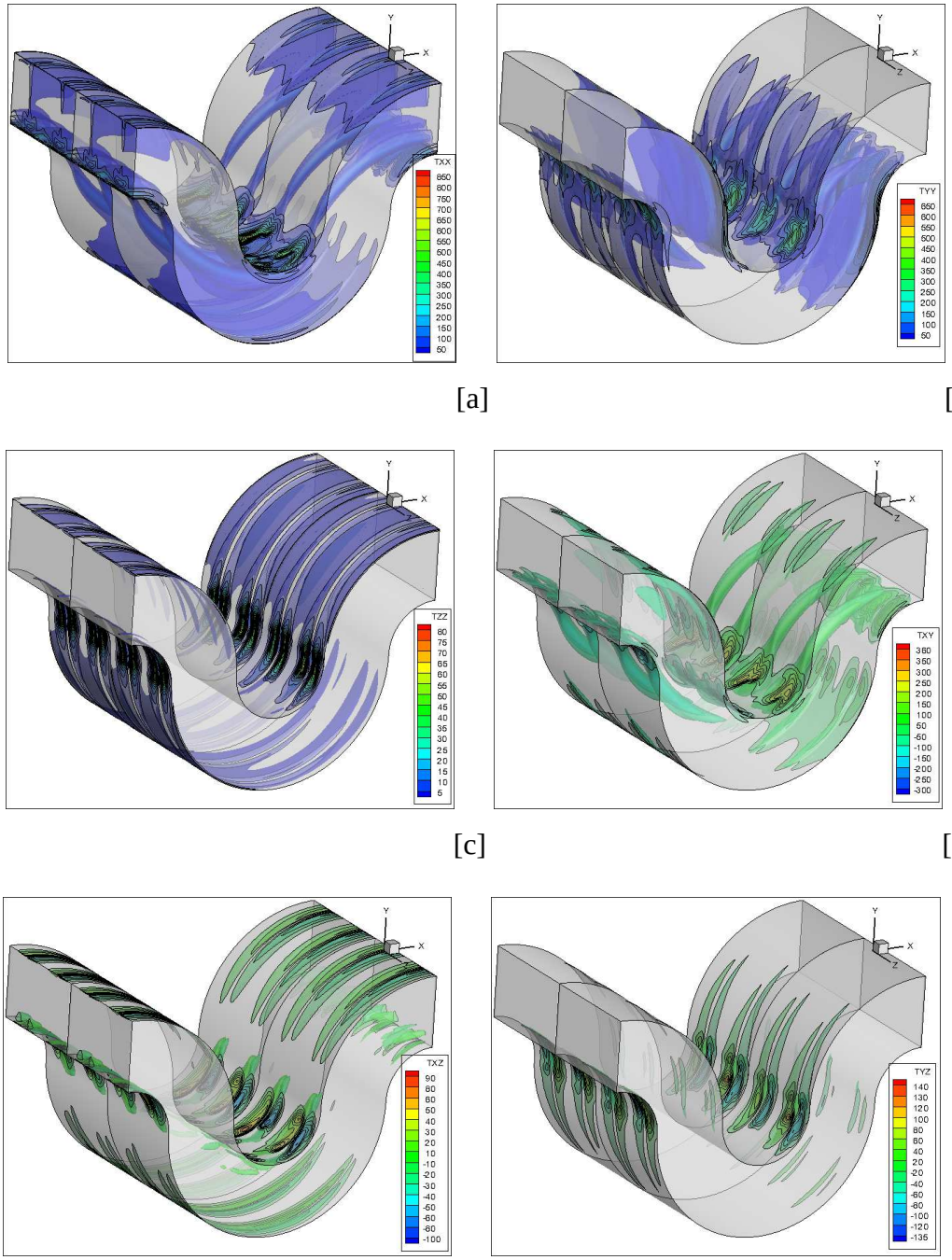

[a] [b]

[c] [d]

[e] [f]

Figure 4.11: The snapshot of the component of the extra stress tensor T_{xx} [a], T_{yy} [b], T_{zz} [c], T_{xy} [d], T_{xz} [e] and T_{yz} [f] for $We = 8$ and $Re = 10$ at $t = 170$.

4.2 Heat Transfer Analysis

Micro heat exchangers are used in many fields of technology; therefore, the heat transfer capabilities of microchannel become important issue. In literature, various enhancement methods have been proposed in order to improve the heat transfer performance of microchannel heat exchanger. It is desirable that the method gives the minimum pressure drop, and the highest heat transfer rate. Therefore, an incompressible viscoelastic fluid has been introduced as a coolant in a micro serpentine channel for heat transfer enhancement.

In this section, the energy equation is solved with the periodic temperature boundary condition with zero temperature jump in the spanwise direction. In streamwise direction, the inflow temperature is rescaled from the temperature at the outflow using the equation (3.66). On the solid walls, the temperature values are equal to zero. The inlet bulk temperature is set to unity. The comparisons between the temperature profile for Newtonian and Oldroyd-B fluid for $Pr = 1$ and $Pr = 10$ are provided in Figure 4.12 and Figure 4.13 for the flow at $We = 0$ and $We = 8$. In order to quantify the heat transfer enhancement, we use the bulk temperature which is defined in equation (3.65) at the outlet of the domain. The comparison of the temperature fields for Oldroyd-B fluid with $Pr = 1$ and $Pr = 10$ is shown in Figure 4.14. In addition, the computed temperature fields for $Pr = 10$ is provided in Figure 4.15. To compare bulk temperature at the outlet, the simulations indicate approximately 20% increase in heat transfer performance at $Re = 10$, $Pr = 10$, $We = 8$. Whalley et al. [21] conducted an experimental study to show that elastic turbulence enhances the heat transfer at the micro-scale geometry as shown in Figure 4.17 by up to 300% under creeping flow conditions. Unlike the serpentine channel used in this study, the length, height and depth of the cross-section was chosen as $6R$, R and R, respectively in dimensionless form where R is the channel minimum radius. The experimental results of Whalley et al. [21] is given in Figure 4.16. By comparing these results with our solution, 20% increase is matching the experimental results.

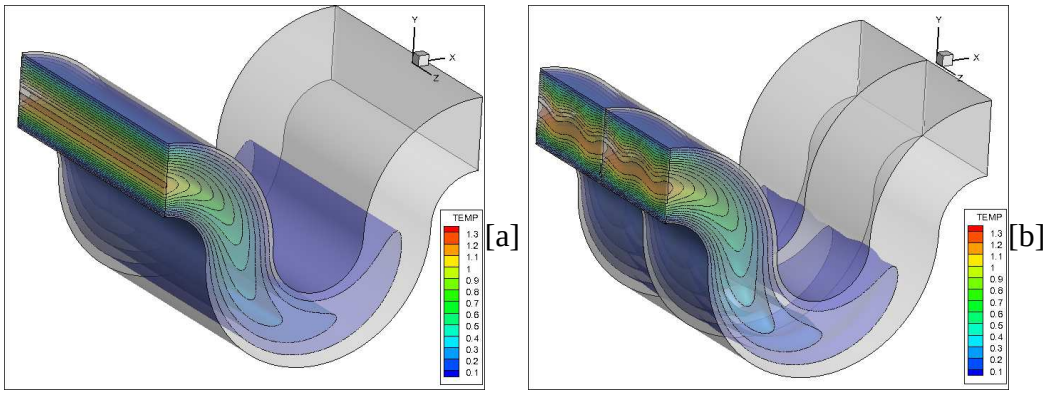

Figure 4.12: The comparison of the temperature for $We = 0$ and $Re = 10$ at $t = 20$ [a] and $We = 8$ and $Re = 10$ at $t = 175$ [b] for $Pr = 1$.

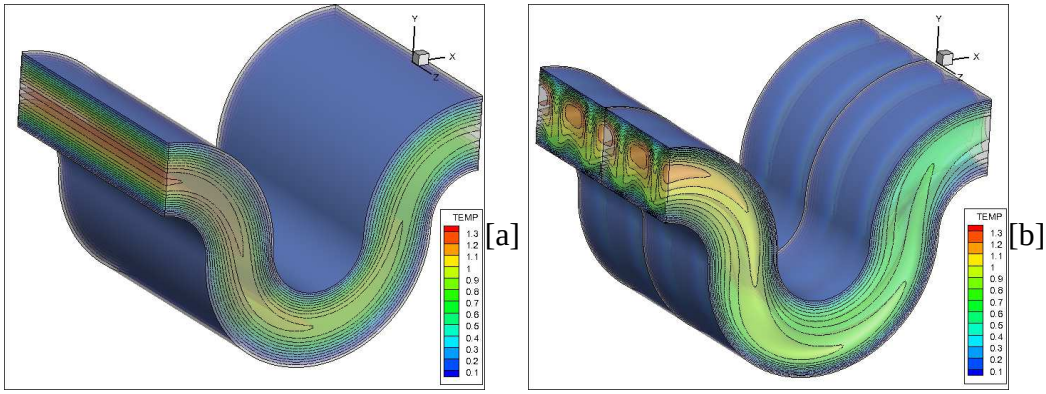

Figure 4.13: The comparison of the temperature for $We = 0$ and $Re = 10$ at $t = 20$ [a] and $We = 8$ and $Re = 10$ at $t = 185$ [b] for $Pr = 10$.

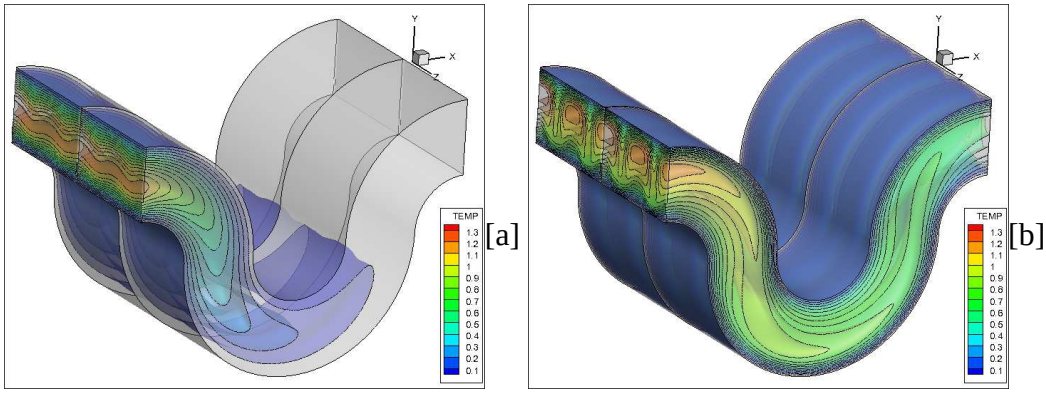

Figure 4.14: The comparison of the temperature for $We = 8$ and $Re = 10$ for $Pr = 1$ [a] and $Pr = 10$ [b] at $t = 175$.

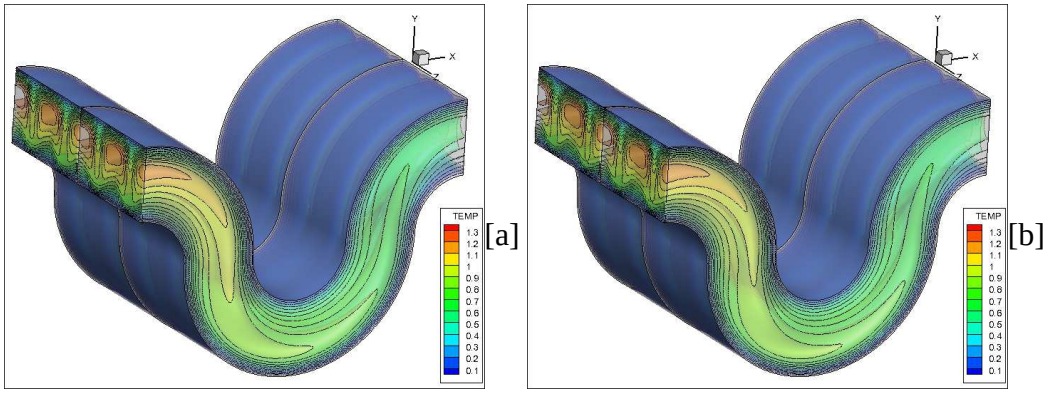

Figure 4.15: The comparison of the temperature for $We = 8$ and $Re = 10$ and $Pr = 10$ at $t = 180$ [a] and at $t = 185$ [a].

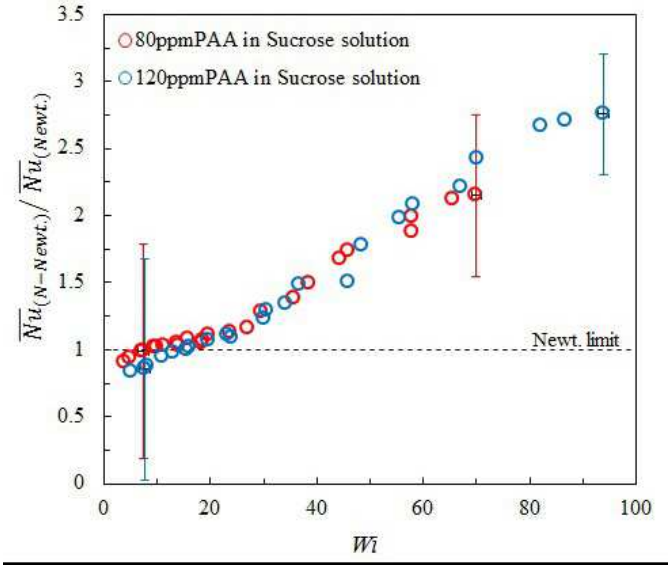

Figure 4.16: Normalized Nusselt number versus Weissenberg number (Wi) [21].

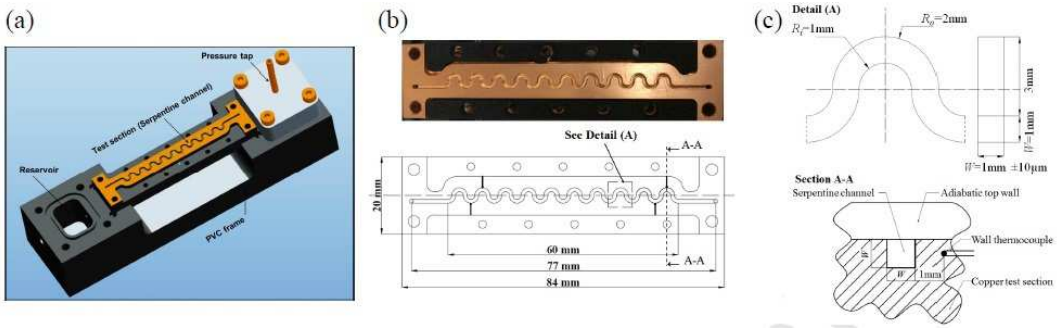

Figure 4.17: Isometric view of the experimental facility (a), plan views of the serpentine channel (b) and detailed view and cross section of the serpentine channel (c) [21].

5. CONCLUSIONS AND FUTUREWORK

Numerical analyses of incompressible fully developed laminar flow of a viscoelastic fluid and heat transfer in serpentine channel which is periodically repetitive in the streamwise and spanwise directions have been carried out using the side-centered finite volume method on unstructured hexahedral meshes. In addition, the simulations are presented for a non-traditional viscoelastic fluid as a coolant in order to enhance heat transfer within a micro serpentine channel. Simulations are performed with Newtonian and viscoelastic (Oldroyd-B) flow. Therefore, the secondary instabilities due to viscoelastic and inertial instabilities are investigated in a micro serpentine duct with rectangular cross section and the strength of the vortices is compared with each other. Then numerical simulations are performed in order to analyze the influence of purely elastic instability on heat transfer enhancement.

The simulations confirm three-dimensional viscoelastic instabilities due to large elastic stresses along the streamlines at vanishingly small Reynolds numbers and the viscoelastic instabilities leads to heat transfer enhancement at higher Weissenberg numbers. The calculations indicate approximately 20% increase in heat transfer performance at $Re = 10$, $Pr = 10$, $We = 8$ and $\beta = 0.67$ compared to that of a Newtonian flow at the same Reynolds number. However, this improvement is accompanied with an increase in pressure jump. It should be noted that the high pressure drop is still problem in microchannels. High pressure drops also lead to an increase in pumping power. In addition, as the Weissenberg number is increased, the viscoelastic instability becomes significant. As a result of this, flow complexity and the strength of vortices increase. Therefore, this secondary flow pattern leads to efficient fluid mixing and high rates of heat transfer. This shows hot fluid being transported away from the walls into the center of the cross section. Moreover, those secondary flows continuously refresh the fluid near the walls and contribute to fluid mixing and heat transfer enhancement.

The simulations are performed to show the influence of the viscoelastic instability on the heat transfer enhancement for $Re = 10$, $We = 8$ compared to that of $Re = 10$,

$We = 0$ which is Newtonian flow. Further numerical studies for $We = 8$ with $Re = 100$ and $Re = 0$, creeping flow, are underway in order to investigate the effect of Reynolds number. It is aimed that heat transfer enhancement will be increased with increasing We number. It should be noted that high We number problem may prevent us to perform simulations at higher Weissenberg numbers. For this purpose, the following items could be investigated as a future work;

- Higher We numbers should be investigated.
- Other boundary condition which is the constant heat flux at wall could be investigated.

REFERENCES

[1] **Gong, L.**, **Kota, K.**, **Tao, W. and Joshi, Y.** (2011). Parametric Numerical Study of Flow and Heat Transfer in Micro channels With Wavy Walls, *Journal of Heat Transfer*, ***133***.

[2] **Volker, S. and Vanka, S.P.** (1997). Fluid Flow and Heat Transfer in Serpentine Channels at Low Reynolds Numbers, *ACRC TR*, ***115***.

[3] **Meis, M.**, **Varas, F.**, **Velázquez, A. and Vega, J.M.** (2010). Heat transfer enhancement in micro-channels caused by vortex promoters, *Int. Journal of Heat and Mass Transfer*, ***53***,*Issues 1-3*, 29–40.

[4] **Toh. K.C.**, **Chen, X.Y. and Chai, J.C.** (2002). Numerical computation of fluid flow and heat transfer in microchannels, *Int. Journal Heat and Mass Transfer*, ***45***, 5133–5141.

[5] **Qu, W. and Mudawar, I.** (2002). Analysis of three-dimensional heat transfer in microchannel heat sinks, *Int. Journal of Heat and Mass Transfer*, ***45***, 3973–3985.

[6] **Qu, W. and Mudawar, I.** (2002). Experimental and numerical study of pressure drop and heat transfer in a single-phase micro-channel heat sink, *Int. Journal of Heat and Mass Transfer*, ***45***, 2549—2565.

[7] **Hartnett, J.P. and Kostic, M.** (1985). Heat transfer to a viscoelastic fluid in laminar flow through a rectangular channel, *Int. J. Heat Mass Transfer*, ***28***, 1147–1155.

[8] **Payvar, P.** (1996). Heat transfer enhancement in laminar flow of viscoelastic fluids through rectangular ducts, *Int. J. Heat Mass Transfer*, ***40***, 745–756.

[9] **Peres, N.**, **Afonso, A.M.**, **Alves, M.A. and Pinho, F.T.** (2009). Heat transfer enhancement in laminar flow of viscoelastic fluids through a rectangular duct, *Congreso de Métodos Numéricos en Ingeniería*.

[10] **Rosaguti, N.R.**, **Fletcher, D.F. and Haynes, B.S.** (2006). Laminar flow and heat transfer in a periodic serpentine channel with semi-circular cross-section, *Int. J. Heat Mass Transfer*, ***49***, 2912–2923.

[11] **Rosaguti, N.R.**, **Fletcher, D.F. and Haynes, B.S.** (2007). Low-Reynolds number heat transfer enhancement in sinusoidal channels, *Chemical Engineering Science*, ***62***, 694–702.

[12] **Poole, R.J.**, **Lindner, A. and Alves, M.A.** (2013). Viscoelastic secondary flows in serpentine channels, *Journal of Non-Newtonian Fluid Mechanics*, ***201***, 10–16.

[13] **Galindo-Rosales, F.J.**, **Campo-Deano, L.**, **Sousa, P.C.**, **Ribeiro, V.M.**, **Oliveira, M.S.N.**, **Alves, M.A. and Pinho, F.T.** (2014). Viscoelastic instabilities in micro-scale flows, *Experimental Thermal and Fluid Science*, ***59***, 128–139.

[14] **Siginer, D.A. and Letelier, M.F.** (2005). Heat Transfer in Laminar Flow of Viscoelastic Fluids in Straight Tubes of Arbitrrary Shape, *Annual Transactions of the Nordic Rheology Society*, ***13***, 137–145.

[15] **Siginer, D.A. and Letelier, M.F.** (2008). Heat Transfer Enhancement, Secondary Flows and Change of Type of Vorticity in non-Circular tube flow of non-Linear Viscoelastic Fluids, *5^{th} European Termal-Sciences Conference*.

[16] **Naccache, M.F. and Souza Mendes, P.R.** (1996). Heat transfer to non-Newtonian fluids in laminar flow through rectangular ducts, *International Journal of Heat and Fluid Flow*, ***17***, *Issue 6*, 613–620.

[17] **Gao, S.X. and Hartnett, J.P.** (1993). Steady Flow of Non-Newtonian Fluids Through Rectangular Ducts, *Int. Comm. Heat Mass Transfer*, ***20***, 197–210.

[18] **Gao, S.X. and Hartnett, J.P.** (1996). Heat transfer behavior of Reiner-Rivlin fluids in rectangular ducts, *Int. J. Heat Mass Transfer*, ***39***,*No. 6*, 1317–1324.

[19] **Syrjala, S.** (1998). Laminar Flow of Viscoelastic Fluids in Rectangular Ducts With Heat Transfer: A Finite Element Analysis, *Int. Comm. Heat Mass Transfer*, ***25***,*No. 2*, 191–204.

[20] **Chang, P.Y.**, **Chou, F.C. and Tung C.W.** (1998). Heat transfer mechanism for Newtonian and non-Newtonian fluids in 2:1 rectangular ducts, *International Journal of Heat and Mass Transfer*, ***41***, 3841–3856.

[21] **Whalley, R.D.**, **Abed, W.M.**, **Dennis, D.J.C. and Poole, R.J.** (2014). Enhancing heat transfer at the micro-scale using elastic turbulence, *Theoretical and Applied Mechanics Letters*, Accepted Manuscript.

[22] **Phillips, R.J.** (1988). Forced-Convection, Liquid-Cooled, Microchannel Heat Sinks, **Technical Report**, ***787***, Lincoln Laboratory.

[23] **Phillips, R.J.** (1988). Microchannel Heat Sinks, *The Lincoln Laboratory Journal*, ***1***, *Number 1*.

[24] **Larson, R.G.** (1992). Instabilities in viscoelastic flows, *Rheologica Acta*, ***31***, 213–263.

[25] **Shaqfeh, E.S.G.** (1996). Purely elastic instabilities in viscometric flows, *Annu. Rev.Fluid Mech.*, ***28***, 129—185.

[26] **McKinley, G.H.**, **Pakdel, P. and Oztekin, A.** (1996). Rheological and geometric scaling of purely elastic flow instabilities, *J. Non-Newton. Fluid Mech.*, ***67***, 19—47.

[27] **Pakdel, P. and McKinley, G.H.** (1996). Elastic instabilities and curved streamlines, *Physical Review Letters*, ***77***, 2459—2462.

[28] **Shah, R.K. and Sekulic, D.R.** (2003). *Fundamentals of Heat Exchanger Design*, John Wiley & Sons, 1–74.

[29] **Kays, W.M. and Crawford, M.E.** (1993). *Convective heat and mass transfer*, McGraw-Hill, 3^{rd} edition, 397–441.

[30] **Strebel K.A.**, (2010). Simulations of Thermophoretic Deposition in Wavy Channels, Master's thesis, The University of Illinois at Urbana, Urbana, Illinois, 3–4.

[31] **Upadhye, H.R. and Kandlikar, S.G.** (2004). Optimization of Microchannel Geometry for Direct Chip Cooling Using Single Phase Heat Transfer, *ASME Micro Channels and Mini Channels*.

[32] **Papautsky, L. and Ameel, T.** (2001). A Review of Laminar Single-Phase Flow in Micro Channles, *ASME International Mechanical Engineering Congress and Exposition*.

[33] **Oldroyd, J.G.** (1949). On the formulation of rheological equations of state, *Proceedings of the Royal Society of London*, ***Series A***, 523–541.

[34] **Sahin, M.** (2011). A stable unstructured finite volume method for parallel large-scale viscoelastic fluid flow calculations, *Journal of Non-Newtonian Fluid Mechanics*, ***166***, 779—791.

[35] **Balay, S.**, **Buschelman, K.**, **Eijkhout, V.**, **Gropp, W.D.**, **Kaushik, D.**, **Knepley, M.G.**, **McInnes, L.C.**, **Smith, B.F. and Zhang, H.** (2004). Petsc users manual, *Anl-95/11, Mathematic and Computer Science Division*, Argonne National Laboratory.

[36] **Karypis, G. and Kumar, V.** (1998). A fast and high quality multilevel scheme for partitioning irregular graphs, *SIAM J. Sci. Computational Mechanics*, ***20***, 359—392.

[37] **Sahin, M. and Wilson, H.J.** (2007). A semi-staggered dilation-free finite volume method for the numerical solution of viscoelastic fluid flows on all-hexahedral elements, *J. Non-Newtonian Fluid Mech.*, ***147***, 79—91.

[38] **Murthy, J.Y. and Mathur, S.** (1997). Periodic Flow and Heat Transfer Using Unstructured Meshes, *International Journal for Numerical Methods in Fluids*, ***25***, 659–677.

[39] **Beale, S.B.** (2007). Use of Streamwise Periodic Boundary Conditions for Problems in Heat and Mass Transfer, *Journal of Heat Transfer*, ***129***, 601–605.

[40] **Patankar, S.V.**, **Liu, C.B. and Sparrow, E.M.** (1977). Fully Developed Flow and Heat Transfer in Ducts Having Streamwise-Periodic Variations of Cross-Section Area, *Journal of Heat Transfer*, ***99***, 180–186.

[41] **Kelkar, K.M. and Patankar, S.V.** (1987). Numerical Prediction of Flow and Heat Transfer in a Parallel Plate Channel With Staggered Fins, *Journal of Heat Transfer*, ***109***, 25–30.

[42] **Niceno, B. and Nobile, E.** (2001). Numerical Analysis of Fluid Flow and Heat Transfer in Periodic Wavy Channels, *Int. Journal of Heat and Fluid Flow*, ***22***, 156–167.

[43] http://picturethis.pnl.gov.

[44] http://dougleschan.com/marine-services-in-singapore/plate-fin-heat-exchanger.

[45] http://trumonyltd.en.made-in-china.com.

[46] http://en.wikipedia.org/wiki/File:AMD_heatsink_and_fan.jpg#file.

CURRICULUM VITAE

Name Surname: Ozan ODUNCU

Place and Date of Birth: Edirne 1989

E-Mail: oduncuozan@itu.edu.tr

B.Sc.: IU Mechanical Engineering

PUBLICATIONS/PRESENTATIONS ON THE THESIS

- Oduncu O., Celik B. and Sahin M., 2015: Heat and Mass Transfer Characteristics of a Micro Serpentine Channel with a Viscoelastic coolant. *8. International Conference on Computational Heat and Mass Transfer*, May 25-28, 2015 Istanbul, Turkey.